EVALUATION OF SHUTTLE IMAGING RADAR DATA FOR DELINEATING AND CHARACTERIZING HIDDEN LANDSCAPES IN SAUDI ARABIA

FINAL REPORT

Submitted To

JoBea Cimino
SIR-B Experiment Scientist
Jet Propulsion Laboratory
Pasadena, California 91109

By

Graydon Lennis Berlin
Department of Geography, Box 15016
Northern Arizona University
Flagstaff, Arizona 86011

March 31, 1989

This report was prepared for the Jet Propulsion Laboratory, California Institute of Technology, sponsored by the National Aeronautics and Space Administration.

ABSTRACT

L-band radar images from the two NASA Shuttle Imaging Radar missions in 1981 and 1984 delineate and characterize a number of different geologic terrains in Saudi Arabia that are completely or partially buried beneath relatively thin deposits of eolian sand. The sand mantle was essentially made transparent because the propagated radar beams were able to penetrate through the fine-grained, loose, and very dry sand deposits and be diffusely reflected from various radar-rough substrates. These buried geologic terrains and landscapes were not amenable to detection by visible and infrared wavelength sensors because they recorded reflected and emitted energies coming totally or primarily from the overburden. Our findings indicate that these unique radar views can provide valuable information for geologic, hydrologic, and archaeologic studies.

INTRODUCTION

The SIR-B Continuation Research Program, entitled "Evaluation of Shuttle Imaging Radar Data for Delineating and Characterizing Hidden Landscapes in Saudi Arabia" and described herein, expands upon two important SIR (Shuttle Imaging Radar) attributes that were previously documented by the Principal Investigator in Saudi Arabia. These attributes were (1) the capability for subsurface imaging and (2) a sensitivity to subtle differences in surface texture or roughness measured at the wavelength scale (i.e., microrelief) (Berlin et al. 1985, 1986). These unique capabilities formed the core of the present investigation that evaluated the utility of SIR-A and SIR-B images for

delineating and characterizing hidden landscapes in three new areas of Saudi Arabia (Figure 1). Hidden landscapes are herewith defined as those older geologic terrains that are not amenable to detection by visible and infrared (VIR) wavelength sensors because of the masking effect of younger eolian surficial deposits (Figure 2).

Studies centered on three different areas where the pre-Quaternary landscapes have been completely or partially buried beneath relatively thin deposits of eolian sand. These areas under study are identified at Sites 1-3 in Figure 1. Reconnaissance field surveys and laboratory analyses of collected samples were fully exploited to determine the physical controls that explained backscatter intensities for exposed, concealed (buried), and obscured (partially buried) landscapes (Figure 2). Geologic interpretation of computer-enhanced Landsat Multispectral Scanner (MSS) and Thematic Mapper (TM) images plus Large Format Camera (LFC) photographs supplemented the investigation.

Two types of special ground measures were needed to fulfill the objectives of the investigation -- determination of microrelief for exposed and obscured surfaces and surface-cover percentages. Measurement of microrelief was accomplished with a wood-dowel templet that depicted height variations over its baselength (Schaber et al. 1980). Its resolution is 1.0-cm horizontal and 0.2-cm vertical. Percentages for surface-cover units were determined by Canfield's (1941) line-interception method.

Results of the research project demonstrate that the L-band SIR images can delineate and characterize both concealed and obscured geologic terrains that are not befit for detection by VIR sensors (Figure 2). Subsurface radar imaging was facilitated because the masking medium (overburden) and buried substrates possessed favorable physical and chemical characteristics that were

amenable to radar penetration, refraction, and reflection during the SIR-A and SIR-B missions in 1981 and 1984. Our findings indicate that the unique SIR views can provide valuable information for geologic, hydrologic, and archaeologic studies, and will perhaps be fully realized when country-wide, L-band radar image coverage is provided by the NASA Earth Observing System.

The Principal Investigator was assisted in the field by Mohammed A. Tarabzouni, Kamel M. Sheikho, and Abdullah H. Al-Naser from the King Abdulaziz City for Science and Technology in Riyadh, Saudi Arabia. All computer image processing tasks and laboratory determinations of grain-size and sorting distributions of collected sand samples were completed by the Principal Investigator at the U.S. Geologic Survey's Flagstaff Field Center in Flagstaff, Arizona, where he serves as a Volunteer Scientist.

BACKGROUND

Saudi Arabia is well suited for subsurface radar imaging because many of its pre-Quaternary geologic terrains are mantled by extensive eolian sand deposits that are normally dry. The eolian veneer is largely the product of two arid phases in the Quaternary Period, including the last 6,000 years or so, when all of Saudi Arabia, except the mountainous southwestern region, has been dominated by eolian erosional and depositional processes (McClure 1976, 1978). In northern Saudi Arabia, extensive areas of the Arabian Shelf's low-rolling sedimentary terrain have been accumulation zones for eolian sand originating from the An Nafud and Ad Dahna sand seas or ergs and from broad areas of poorly consolidated Paleozoic sandstones that are exposed in northwestern Saudi Arabia. In addition, large areas of the Arabian Shield are

veneered by thin, windblown sand deposits. Representative types of Quaternary eolian cover include sand sheets or blankets, sand drifts, sand shadows, small dune fields, and paleowadi fill-sand.

The three areas of investigation lie in arid and hyperarid bioclimatic zones that are characterized by precipitation/potential evapotranspiration ratios (P/Etp) of 0.03 to 0.2 and less than 0.03, respectively (UNESCO 1977). Mean annual precipitation is less than 120 mm. Rainfall, although unpredictable and irregular, occurs predominantly during the months between December and March. This winter maxima is extremely important because the SIR-A and SIR-B missions occurred in late fall, a time when the moisture content of the sand deposits was at minimum levels. Because of the sparcity of rainfall, natural vegetation is restricted to scattered xerophytic shrubs and seasonal grasses.

RATIONALE FOR THE CONTINUATION PROJECT

The SIR-A/SIR-B Continuation Project was initiated because our earlier research in Saudi Arabia had demonstrated the subsurface imaging capability of both SIR-A and SIR-B for an extensive area along the southern margin of the Al Labbah Plateau (Berlin et al. 1985, 1986). The study area is shown as Site #4 in Figure 1. The SIR-A image of the study area is presented in Figure 3, while computer-enhanced Landsat TM images are presented in Figures 4 and 5.

The local area is dominated by three eolian sand features: (1) a 37-m high sand hill called Anbat, (2) an elongated sand shadow (two wings) called Irq al Ubaytir, and (3) the informally named Al Labbah sand sheet (Figures 3-5). Both the SIR-A and SIR-B beams penetrated through the widespread sand

sheet and were diffusely reflected from the buried and radar-rough Aruma Formation, which is primarily a shallow-water limestone (Powers et al. 1966). A surface view of the penetrated sand sheet is shown in Figure 6. Depth measurements from more than 80 test holes excavated in the sand sheet show that subsurface imaging had occurred through a sand layer whose maximum measured thickness is 1.24 m.

Within the areal bounds of the penetrated sand sheet, the SIR-A image dramatically defines the thick sand deposits at Anbat and Irq al Ubaytir (Figure 3). These features are depicted as a dark tone in the SIR-A image because the radar signal was either unable to penetrate through their thicker sand layers to the reflecting substrate, or to exit the sand layer after subsurface reflection. The minimum thickness where subsurface imaging did not occur is estimated to be about 3.1 m; this occurred along the southern wing of Irq al Ubaytir (Figures 3 and 7).

STUDY AREA RESULTS

The present investigation centered on three targeted areas (1) where different degrees of surficial masking were known to exist and (2) where it appeared that there was either SIR-A or SIR-B signal penetration to a radar-rough substrate. Two of the targeted sites are located on the Arabian Shelf and include extensive paleodrainage systems. The Al Khunfah Plateau study area (center coordinates: 28° 30'N, 39° 30'E) is shown as Site #1 in Figure 1, and the Al Labbah Plateau study area (center coordinates: 29° 10'N, 42° 10'E) is shown as Site #2 in Figure 1. The third study area centers on the Harrat Hutaymah at the east-central margin of the Arabian Shield (center coordinates: 27°N, 42° 20'E); it is shown as Site #3 in Figure 1.

Ground surveys have identified two states of surficial material masking for the three study areas. In one case, the older geologic terrain is invisible over large areas because of its complete burial by windblown sand deposits; this condition produces what we call a concealed or buried landscape (Figure 2). For the second case, the geologic terrain is identifiable by direct field observation because sporadic outcrops can be seen protruding through the sand cover; this degree of masking is responsible for producing an obscured or partially buried landscape (Figure 2). Both total and partial masking can produce opaque or "blind" conditions for VIR sensors because of their inability to detect the subsurface. The term hidden landscape has been coined to encompass both the concealed and obscured states of terrain burial (Figure 2).

Because of SIR's subsurface imaging capability, the eolian cover is rendered essentially transparent under the correct conditions. Thus, in contrast to the VIR sensors, the SIR systems are capable of detecting both types of hidden landscapes (Figure 2). Both SIR and VIR sensor systems can detect exposed landscapes (Figure 2).

From a remote sensing perspective, concealed or buried geologic terrains cannot be detected by VIR sensors because they provide information about reflectance and emittance properties of the surface material, in this case those of the overburden. Based upon our field measurements, it has been determined that a partially buried geologic terrain (i.e., obscured landscape) can assume the characteristics of a buried landscape for VIR sensors when the amount of surficial material cover exceeds about 60 percent of the ground resolution cell. In this state, the VIR return signal is essentially determined by the reflectance and emittance properties of the surficial material. SIR backscatter or echo intensity, by comparison, is determined by

both the surface and subsurface components of the radar-rough, geologic terrain unit, with no appreciable input from the surficial overburden (Figure 2).

Al Khunfah Plateau Study Area

The ability of SIR-A to detect both buried and partially buried landscapes is illustrated at the Al Khunfah Plateau study area (Site #1 in Figure 1). The SIR-A image and LFC photograph of the local region are presented in Figure 8.

The Al Khunfah Plateau is an undulating plain that is underlain by the virtually flat-lying Tawil sandstone of Devonian age (Powers et al. 1966). The Tawil is a coarse, crossbedded sandstone that weathers to a rough, slabby surface (Lambertian type). Protected outcrops are normally coated with grayish black (Munsell notation = N2) desert varnish; ablated outcrop surfaces are free of varnish and have colors ranging from very pale orange (Munsell notation = 10YR 8/2) to light brown (Munsell notation = 5YR 4/4).

Extensive areas of the Al Khunfah Plateau are now covered by various thicknesses of loose drift sand, punctuated with local barchanoid dunes (Figures 9 and 10). The eolian sand is derived principally from broad areas of poorly consolidated Paleozoic sandstones that are exposed to the west of the local region. The color of the drift sand varies from reddish yellow (Munsell notation = 10YR 6/6) to dark yellowish orange (Munsell notation = 10 YR 6/6). The color of the dune sand is commonly pale yellowish orange (Munsell notation = 10YR 8/6). The sand deposits are predominantly composed of quartz grains with trace amounts of potassium feldspar and heavy minerals. Grain-size analyses for two collected sand samples are presented in Table 1 (Sites 1 and 2 in Figure 8).

A feature of special interest is the aggraded Wadi Nayyal paleodrainage system (master stream and tributaries from local drainage basins) that was carved into the plateau's sandstone strata by intensive runoff that occurred during late Tertiary and early Quaternary pluvials (Figure 8). The defunct Wadi Nayyal has a maximum width of approximately 5 km; its contemporary bed surface is from 10 to 40 m below the adjacent upland surface (Figure 11). The small tributary wadis to the east of Wadi Nayyal have widths as narrow as 15 m; most of their bed surfaces are from 3 to 10 m below the adjacent remnant interfluves (Figures 9 and 10).

The dry wadi beds are surfaced with one or more of the following types of surficial deposits: (1) late Tertiary stream-rounded and ferruginous stained gravel; (2) locally-derived Quaternary alluvium consisting of unconsolidated silt, sand, and gravel; and (3) eolian wadi-fill sand of Quaternary age (Figures 9-12). The latter type of deposit is especially common because many of the relict wadi channels have acted as efficient sand traps throughout the late Quaternary on account of their negative topographic expression and their transverse orientation to the prevailing wind direction (Figures 9-11).

Comparison of the SIR-A image and LFC photograph indicates that each portrays a dramatically different view of the study area (Figure 8). The LFC photograph shows a contemporary terrain dominated by eolian sand deposits, while the SIR-A image reveals a predominantly paleo-fluvial terrain. The paleo-fluvial terrain is clearly defined in the SIR-A image because (1) varying thicknesses of drift sand overlying the Tawil sandstone on the remnant interfluves were penetrated by the propagated beam (bright image tones), and (2) the wadi beds were responsible for a minimal backscatter component (dark image tones) because the incident beam was largely reflected from their radar-smooth surfaces in a mirror-like fashion (i.e., away from the antenna) and/or

attenuated in the channel fill (Figure 12). The maximum measured sand depth for a concealed landscape is 36 cm (Site A in Figure 11). The LFC photograph shows little tonal contrast between the remnant interfluves and wadi beds because their sand veneered surfaces did not produce distinctive signatures at visible wavelengths (Figures 8-11).

Al Labbah Plateau Study Area

The ability of SIR-B to detect a partially buried or obscured landscape is illustrated at the Al Labbah study area (Site #2 in Figure 1). The computer-enhanced SIR-B image and an accompanying computer-enhanced Landsat MSS band 7 image are presented in Figures 13 and 14, respectively. The SIR-B digital image was subjected to a 3 x 3 pixel, median-value filter operation to reduce speckle noise and a special algorithm developed by Chavez and Berlin (1986) to suppress across-track radiometric noise that was associated with certain SIR-B digital images. The MSS band 7 image was subjected to a high-pass filtering operation to enhance high-frequency spatial information; the filter size was 101 x 101 pixels (Avery and Berlin 1985). Both images incorporate linear stretches to increase scene contrast while preserving original radiance and backscatter relationships.

The local area is underlain by flat-lying carbonate rocks of the Upper Cretaceous Aruma Formation (limestone and subordinate dolomite) (Powers et al. 1966). The terrain is gently rolling and is indented by the relict Wadi Al Khirr drainage system. The exposed surface of the Aruma Formation is commonly littered with angular rock fragments that vary in size from pebbles to cobbles, with varying concentrations of boulders (Figure 15). The rocks range in color from pale brown (Munsell notation = 5YR 5/2) to very pale orange (Munsell notation = 10YR 8/2).

Under the arid to hyperarid conditions that have persisted for the past 5,000 to 6,000 years, widespread areas of the plateau, including the transverse wadi systems, have been veneered with discontinuous eolian sand deposits supplied principally from the An Nafud sand sea (Figures 16 and 17). The sand is predominantly composed of quartz grains (about 97 percent), with minor amounts of potassium feldspar, dolomite, and heavy minerals. Isolated quartz aggregates (calcium-carbonate cement) were also present. Grain-size analyses for upland and wadi sand samples are presented in Table 1 (Sites 2 and 4 in Figures 13 and 14). The color of the eolian sand ranges from reddish yellow (Munsell notation = 5YR 6/8) to yellowish red (Munsell notation = 5YR 5/8).

The local area is dominated by the Wadi Al Khirr paleodrainage system. The defunct Wadi Al Khirr has a width of about 2 to 3 km, and its contemporary bed surface is approximately 100 m below the adjacent remnant interfluves (Figure 18). Wadi Al Khirr drained northward during late Tertiary and early Quaternary pluvials from the Arabian Shield, across the Arabian Shelf, to the Tigrus-Euphrates system. In the local study area, the wadi is about 300 km from its original catchment area in the Arabian Shield and much of its lower course now disappears beneath the Ad Dahna sand sea (Figures 13 and 14). Under the present hyperarid conditions, the Wadi Al Khirr system effects only local drainage from episodic rainfall events. During our ground surveys, we encountered a number of Neolithic sites within and along the upland margins of Wadi Al Khirr and its tributaries; a discussion centering on the wadi system as a prehistoric ecological niche is presented in a later system.

Analogous to the Al Khunfah study site (Figure 8), the SIR-B and MSS band 7 images provide different perspectives of the same ground area. In the MSS image, for example, Aruma Formation outcrops have relatively dark signatures,

while the eolian sand deposits are depicted in bright tones (Figures 14 - 17). This is attributable to significant differences in their reflective properties at near-infrared wavelengths. The tonal category for the eolian sand is associated with both upland surfaces and wadi floors. Consequently, it is difficult to differentiate these two terrain elements solely on the basis of image tone. This is especially true for the wadis sited to the west of Wadi Al Khirr.

In the MSS image, the lateral boundaries of Wadi Al Khirr are definable only along those segments where Aruma outcrops are exposed, or where there is shadow/highlight enhancement of valley walls (Figure 14). On the published, 1:500,000-scale geology map (Bramkamp and Ramirez 1963), these are the only segments of Wadi Al Khirr that are delineated. Elsewhere along the wadi course, the masking sand deposits undoubtedly caused an identification problem because heavy reliance was placed on the interpretation of small-scale aerial photographs. The segments of Wadi Al Khirr at Sites 4 and 5 in Figures 13 and 14 were not mapped (Bramkamp and Ramirez 1963).

In the SIR-B image, the bright tonal signatures for the rubbly outcrops of the Aruma Formation are attributable to strong intensity returns because their rough surfaces (Lambertian type) directly reflected a large proportion of the incident signal back to the antenna (Figures 13 and 15). The partially buried Aruma Formation (Figures 13, 16 - 17) is depicted in slightly darker tones than its surface counterpart. Two reasons, either singularly or in combination, could explain the diminuation in tone---its roughness is subdued or signal attenuation occurred in the two-way travel path through the penetrated sand deposits.

The wadi beds were responsible for a minimal backscatter component because the incident radar signal was largely reflected from their smooth

surfaces in a single direction away from the antenna (i.e., Fresnel-reflection direction) and/or attenuated in the channel fill (Figures 13 and 18). Consequently, the wadis are clearly discernable in the SIR-B image as dark toned features in juxtaposition with lighter toned upland surfaces (Figure 13).

Harrat Hutaymah Study Area

The ability of SIR-A to detect two, sand-obscured lava flows is illustrated at the Harrat Hutaymah study area, which is located at the east-central margin of the Arabian Shield (Site #3 in Figure 1). The local region is underlain by a varied assemblage of Proterozoic plutonic, metavolcanic, and metasedimentary units. The Proterozoic rocks are commonly overlapped disconformably by basaltic cinder cones, tuff rings, and lava flows of Quaternary age that comprise the Harrat Hutaymah volcanic field. Surficial eluvial deposits of Quaternary age are extensive and include sheet gravel deposits, wadi alluvium, sabkha deposits, and eolian sand (William et al. 1986).

Our area of concentration centered on two, flat-lying lava flows within Harrat Hutaymah--the informally named Najafat Umm Harruj and Ath Thu'aylibi lava flows (Features A and B in Figure 19). Both flows have exposed and sand-masked surfaces. The exposed aa flow segments are fractured with very rugged surfaces (Figures 20 and 21). Based upon Fisher's (1961) classification scheme, most of the pyroclastic fragments are blocks (>64 mm) with a minor amount of lapilli (2-64 mm). When varnished, the fragments have surface colors ranging from brownish black (Munsell notation = 5YR 4/1) to brownish gray (Munsell = 5YR 4/1). Unvarnished fragments have dark gray (Munsell notation = N3) and medium dark gray (Munsell notation = N4) surfaces.

Quartzose sand (minor content of basaltic clasts), and primarily of eolian origin, has accumulated in the pockets or micro-depressions over most of the Ath Thu'aylibi flow surface and the western portion of the Najafat Umm Harruj flow surface (Figure 19). The sand ranges from a few centimeters in thickness to a maximum measured depth of about 35 cm and has effectively caused a smoother flow-surface. The sand varies in color from very pale brown (Munsell notations = 10YR 7/3 and 7/4) to pinkish gray (Munsell notation = 7.5YR 7/2). Grain-size analyses for three collected samples are presented in Table 1 (Sites 3, 4, and 6 in Figure 19). Percentages of sand cover for five sites are presented in Table 2 (Sites 3-7 in Figure 19). Ground views of two sand-obscured sites are presented in Figures 22 and 23.

When observed from the air, large segments of the sand-obscured terrain are difficult to recognize as actual flow surfaces when evaluated solely on the basis of their color signatures (Figures 24-26). Most segments can be identified as flow surfaces, however, if their bounding flow margins are visible (i.e., free of deposited particles), or if their topographic position is considered.

Both the exposed and sand-obscured flow surfaces are clearly seen on the SIR-A image, with the exposed unit being depicted in lighter tones than the sand-obscured unit (Figure 19). Both flow types are easily discriminated from their eluvial surroundings, which are depicted in dark signatures. These discriminations were also quantitatively defined by DN (digital number) statistics that were computed from a digitized version of the SIR-A image (Table 3).

A question that we wanted to answer was the following: Are the tonal classes of the exposed and obscured lava surfaces in agreement with the solutions of the modified Rayleigh criterion (Peake and Oliver 1971)? The

smooth criterion considers a surface to be radar smooth, and hence dark toned on a radar image, when

$$h < \frac{\lambda}{25 \sin \beta} \qquad (1)$$

where h = average vertical height of microrelief, λ = operating wavelength, and β = antenna depression angle. The rough criterion considers a surface to be radar rough, and hence light toned on a radar image, when

$$h > \frac{\lambda}{4.4 \sin \beta} \qquad (2)$$

Surfaces with a roughness falling between the upper and lower limits will be responsible for an intermediate radar return, and hence mid graytones on a radar image.

Using a 23.5-cm SIR-A wavelength and a depression angle of 39° for the area of the two lava flows, the smooth and rough criteria equal 1.49 and 8.49 cm, respectively. A surface of intermediate roughness would have values falling between these two calculated boundaries. Such a surface would produce an intermediate radar return, which would be rendered as medium gray signatures in the image.

Our templet determinations of mean surface relief show good agreement with the tonal depiction of the exposed lava surfaces (Sites 1 and 2 in Figure 19). The mean relief for these two surfaces equal 8.59 and 8.04 cm (Table 2). The high returns from their surfaces were caused by single reflections from properly oriented facets of the large, loose blocks (Figures 20 and 21).

The templet determinations of mean surface relief for the five sand-veneered flow surfaces fall into, or lie very close to, the smooth criterion

(< 1.49 cm) (Sites 3-7 in Figure 19 and Table 2). This would indicate that the surfaces should be depicted in dark signatures, but not intermediate gray tones as was the actual case (Figure 19). This implies that the L-band energy was reflected from not only the exposed pyroclastic fragments, but also from sand-buried lava blocks. Thus, the surficial cover was rendered essentially transparent by the SIR-A beam (Sites 3-7 in Figure 19).

To ascertain the ability of Landsat MSS and TM images to depict the sand-obscured flow surfaces, several computer-processed color composites were produced for visual analysis. The MSS and TM data bases were first corrected for atmospheric haze effects by Chavez's (1988) dark-object subtraction technique. The MSS color composites included (1) simulated natural color (Eliason et al. 1974), (2) color infrared (bands 4, 5, and 7), incorporating linear contrast stretches, and (3) false color (bands 4, 5, and 7), incorporating sinusoidal ("sine") contrast stretches (Avery and Berlin 1985). These images are presented in Figure 27. The TM color composites that were produced included the following types: (1) three band composites, (2) three band-ratio composites, (3) decorrelation stretched band composites (Gillespie et al. 1986), and (4) principal component band composites. Those having the best discrimination qualities are presented in Figures 19 and 28.

On the computer-enhanced MSS and TM images, the sand-veneered top of the western margin of the Najafat Umm Harruj flow cannot be separated from its eluvial/pediment surroundings (Figures 19, 27-28). However, certain segments of the flow front are identifiable on the TM color ratio composite and principal component composite (Figure 28). This enhancement was likely caused by the lack of sand cover along portions of the flow front. A portion of this sand-free zone (western most margin) is observable in the oblique airphoto that is presented in Figure 24.

On most of the MSS and TM images, it is possible to separate the sand-veneered Ath Thu'aylibi flow from its eluvial/pediment surroundings (Figures 19, 27-28). This is possible, not because of differences in its color rendition versus background, but primarily because the images capture most of its steep lateral margins, which are largely devoid of sand. This narrow zone generally contrasts vividly with the immediate surroundings (Figures 19, 27-28).

Within the overall flow surface of Ath Thu'aylibi, the TM images tend to show a slight signature difference between the eastern and western halves of the flow (Figures 19, 27-28). Our surface measurements show that the western sector of the flow has a slightly higher percentage of sand cover (Table 2). The SIR-A image displays both flow segments in identical tones (Figure 19).

On the published, 1:250,000-scale geologic map for this region (Williams et al. 1986), only portions of the sand-masked surfaces were mapped as actual flow surfaces. For instance, a considerable portion of the western lobes of the Najafat Umm Harruj and Ath Thu'aylibi flows were mapped as Quaternary alluvium and Proterozoic quartz diorite. The masking sand deposits undoubtedly caused an identification problem because field mapping was done with the aid of 1:60,000-scale airphotos and 1:250,000-scale Landsat MSS images (Williams et al. 1986). If the SIR-A image would have been available, it is likely that the entire surfaces for both flows would have been identified and mapped.

GROUND CONDITIONS FAVORING SUBSURFACE IMAGING

Several favorable ground conditions, working simultaneously and in conjunction with desirable SIR system characteristics (e.g., L-band wavelength, HH polarization, and relatively large look angles), provided an environment conducive for signal penetration in the study areas during the SIR-A and SIR-B missions. These conditions were as follows:

(1) The moisture content of the sand deposits is assumed to have been below the critical 1 percent level (Blom et al. 1984) during the SIR-A and SIR-B missions. Weather records indicate that the study areas had been without precipitation for at least six months prior to the Shuttle overflights in November 1981 and October 1984. Specifically, at the Al Labbah study area (Site #4 in Figure 1), the moisture level averaged only 0.21 weight percent for sand samples collected at the surface and at two subsurface levels (three determinations per site) on the day of the SIR-B overpass. Such a diminished value describes a low loss medium that would permit the SIR signals to penetrate to a relatively deep depth without significant dispersion.

(2) The individual grains of the sand deposits were too small to scatter the large wavelength radar signals. Roth and Elachi (1975) found that scattering losses are not prohibitive for subsurface penetration when individual grain sizes are smaller than one-tenth wavelength, and that scattering losses do not become appreciable until grain sizes become larger than one-fifth wavelength. With a SIR wavelength of 23.5 cm, the critical grain-size values are 2.35 and 4.70 cm, respectively. The mean grain size of sand samples at the Al Labbah, Al Khunfah, and Harrat Hutaymah study sites (Sites 1-3 in

Figure 1) averaged 0.3 mm (n = 7), or slightly more than one-thousandth of the wavelength (Table 1).

(3) The quartose sand deposits were essentially devoid of clay minerals. Water-bearing minerals can severely attenuate radar signals, and thus drastically restrict signal penetration (Schaber et al. 1986).

(4) The sand deposits did not contain buried inhomogeneities (e.g., coarse gravel layer, hardpan, duricrust) that would have prevented the radar signals from reaching a hidden landscape surface. If present, any subsurface backscatter would have been from the "suspended" interface and not from the buried geologic-terrain surface.

(5) The hidden landscape surfaces were radar rough, and they thus diffusely reflected the radar signals. If a buried substrate had been radar smooth, the propagated signals would have been specularly reflected away from the antenna, and there would have been no image evidence (i.e., signal modulation) of a subsurface landscape.

(6) The masking sand layers were thin enough to enable the radar signals to penetrate to a rough substrate and be reflected back through the low loss medium. If the surficial deposits had been excessively thick, the radar energy would have been converted to heat energy somewhere along the two-way travel path.

(7) With only sparse vegetation covering the sand deposits, there was an insufficient number of surface-point scatterers to diffusely reflect the

propagated radar signals at the air-sand interface. As a consequence, essentially all of the radar energy was available for penetration, with echo intensity being determined by the buried substrate.

SAND DEPOSITS AND BACKSCATTER ENHANCEMENT

The presence of a thin layer of dry sand could have enhanced the ability of SIR-A and SIR-B to image buried and partially buried substrates because of (1) refraction of the propagated radar beam at the air-sand interface, effectively producing a steeper or smaller incidence angle at the sand-bedrock interface (Figure 29), and (2) effective wavelength shortening in the penetrated medium. The smaller incidence angle and shorter wavelength would increase the backscatter, which would help compensate for any radar absorption losses in the sand and any specular reflection that occurred at the air-sand interface (Elachi et al. 1984).

Without an overburden, the relationship between wavelength and incidence angle establishes the theoretical boundary between smooth and rough surfaces. The Rayleigh criterion considers a surface to be smooth if:

$$h < \frac{\lambda}{8 \cos \theta} \qquad (3)$$

where: h = average vertical relief of surface roughness (cm)

λ = operating radar wavelength (cm)

θ = incidence angle of the radar beam

By solving for h in Equation 3, the theoretical boundary of vertical relief separating radar-smooth and radar-rough surfaces is defined for a given

wavelength and incidence angle. Accordingly, surfaces with a value of h less than the calculated value should produce dark image tones (radar-smooth surfaces), and surfaces with a value of h greater than the calculated value should be responsible for light image tones (radar-rough surfaces). With SIR-A, for example, with a wavelength of 23.5 cm and an incidence angle of 47°, an average vertical relief of 4.3 cm is the theoretical boundary between smooth and rough surfaces.

However, given the condition of a sand-covered substrate, the Rayleigh criterion assumes the following form because of wave refraction (Elachi et al. 1984; McCauley et al. 1982):

$$h' < \frac{\lambda'}{8 \cos \theta'} \qquad (4)$$

where: h' = apparent average vertical relief of subsurface roughness

$\lambda' = \lambda/\sqrt{\xi}$ with ξ being the complex dielectric constant of the penetrated medium

$\theta' = \arcsin([\sin \theta]/\sqrt{\theta})$

By using appropriate SIR-A values and $\xi = 2.5$, which was the mean complex dielectric constant of surface and subsurface sand samples collected during the dry season at the Al Labbah Plateau study site (Site #4 in Figure 1), the parameters for Equation 4 are as follows: (1) the surface wavelength (λ) of 23.5 cm is reduced to a subsurface wavelength (λ') of 14.9 cm; (2) the surface incidence angle (θ) of 47° becomes 27.5° at the air-sand interface (θ'); and (3) the theoretical boundary between radar smooth and radar rough would have gone from 4.3 cm at the surface (h) to 2.1 cm at the subsurface (h'). Thus, with h' less than 2.1 cm, the rubble surface of the buried rocks of the Tawil sandstone and Aruma Formation, for example, would clearly represent a radar-rough surface (Figure 15).

CONCLUSIONS

Our investigation has shown that L-band SIR images can delineate and characterize both concealed and obscured geologic terrains (i.e., hidden landscapes) that are not befit for detection by VIR sensors. Surface radar imaging was facilitated because the masking medium (overburden) and buried substrates possessed favorable physical and chemical characteristics that were amenable to radar penetration, refraction, and reflection during the SIR-A and SIR-B missions.

Although SIR-A and SIR-B provided only limited image coverage of Saudi Arabia, the unique radar views of several terrains do illustrate their potential for important applications in geology, hydrology, and archaelogy. For example, the SIR images could be used effectively to assist the field geologist in mapping lithologic units and terrain features (e.g., drainage networks) in areas that veneered by thin windblown sand deposits. A problem created by surficial masking is demonstrated on published 1:500,000-scale and 1:250,000-scale geology maps, where the level of detail is conspicuously generalized in sand-veneered areas because heavy reliance had to be placed on the interpretation of 1:250,000-scale Landsat MSS images and/or 1:60,000-scale panchromatic airphotos. We have found that in such areas, SIR interpretive data could be used to revise the existing maps by correcting errors and adding terrain information.

The ability of the SIR sensors to detect paleo-fluvial terrains has important applications in both hydrology and archaeology. For example, the relic alluvial valleys that formed during past humid periods could be

favorable sites for shallow groundwater occurrence because they may contain large water-bearing beds that could be recharged if the paleodrainage systems are still in hydraulic communication with their original catchment areas in the Arabian Shield. The same paleodrainage systems are also considered to be favorable ecological niches for Stone Age and Neolithic settlements. During our survey work, for example, we discovered a number of MAR-TU stone-"kite" structures (animal traps) along the margins of many of the relic valleys, including Wadi Al Khirr (Figure 30); these structures were used from about 6,000 B.C. to 2,000 B.C. (Zarins 1986).

Being able to detect hidden landscapes with L-band SIR sensors expands the role of remote sensing as a tool for problem solving in the earth sciences. For Saudi Arabia and other countries that have been dominated by eolian depositional activities throughout the late Quaternary Period, the unique radar views could become fully exploitable when country-wide, L-band image coverage is provided by the NASA Earth Observing System (EOS) that is planned to be operational by the late 1990's.

To date, the Principal Investigator has presented the results of this investigation (oral presentation) at the Symposium on Space Commercialization: Roles of Developing Countries (March 5-10, 1989; Nashville, TN). The Symposium was sponsored by the University of Tennessee Space Institute, United Nations, American Institute of Aeronautics and Astronautics, and the International Academy of Astronautics. Also, a manuscript entitled "Detection of Hidden Landscapes in Saudi Arabia with Shuttle Radar Images" has been accepted for publication in the American Institute of Aeronautics and Astronautics Journal. A copy of this manuscript is found at the end of the Final Report.

The Principal Investigator is currently preparing a manuscript entitled "Shuttle Radar Imagery and Paleo-Drainage Systems in North-Central Saudi Arabia: Ecological Niches for the Neolithic MAR-TU Pastorialists." This manuscript will be submitted to the Journal of Field Archaeology. An oral or poster presentation on this same topic is also planned for the 55th Annual Meeting of the Society for American Archaeology.

Lastly, the Principal Investigator is preparing a manuscript entitled "Shuttle Imaging Radar Detection of Partially Buried Lava Flows in Harrat Hutaymah, Saudi Arabia." This manuscript will be submitted to either Remote Sensing of Environment or Geocarto International. In each of the above cases, reprints will be sent to the appropriate individuals at JPL and NASA as soon as they become available.

REFERENCES

Avery, T. E. and G. L. Berlin, 1985, Digital Image Processing, (in) Interpretation of Aerial Photographs, Macmillan Pub. Co., New York, 4th ed., pp. 451-536.

Berlin, G. L., M. A. Tarabzouni, K. M. Sheikho, and A. H. Al-Naser, 1985, SIR-A and Landsat MSS observations of eolian sand deposits on the Al Labbah Plateau, Saudi Arabia, in Proceedings, Nineteenth International Symposium on Remote Sensing of Environment, Environmental Research Institute of Michigan, Ann Arbor, Vol. 1, pp. 321-331.

Berlin, G. L., M. A. Tarabzouni, A. H. Al-Naser, K. M. Sheikho, and R. W. Larson, 1986, SIR-B subsurface imaging of a sand-buried landscape: Al Labbah Plateau, Saudi Arabia, IEEE Transactions on Geoscience and Remote Sensing, Vol. GE-24, pp. 595-602.

Blom, R. G., R. E. Crippen, and C. Elachi, 1984, Detection of subsurface features in SEASAT radar images of Means Valley, Mojave Desert, California, Geology, Vol. 12, pp. 346-349.

Bramkamp, R. A. and L. F. Ramirez, 1963, Geology of the Darb Zubayah Quadrangle, Kingdom of Saudi Arabia, Map I-202A, U.S. Geological Survey, scale 1:500,000.

Canfield, R., 1941, Application of the line interception method in sampling range vegetation, Journal of Forestry, Vol. 39, pp. 388-394.

Chavez, P. S., Jr., 1988, An improved dark-object subtraction technique for atmospheric scattering correction of multispectral data, Remote Sensing of Environment, Vol. 24, pp. 459-479.

Chavez, P. S., Jr. and G. L. Berlin, 1986, Computer restoration techniques for SIR-B digital radar images, in Proceedings, Fifth Thematic

Conference: Remote Sensing for Exploration Geology, Environmental Research Institute of Michigan, Ann Arbor, pp. 501-511.

Elachi, C., L. R. Roth, and G. G. Schaber, 1984, Spaceborne radar subsurface imaging in hyperarid regions, IEEE Transactions on Geoscience and Remote Sensing, Vol. G. E.-22, pp. 383-388.

Eliason, E. M., P. S. Chavez, Jr., and L. A. Soderblom, 1974, Simulated "true color" images for ERTS data, Geology, Vol. 2, pp. 231-234.

Fisher, R. V., 1961, Proposed classification of volcaniclastic sediments and rocks, Geological Society of America Bulletin, Vol. 72, pp. 1409-1414.

Gillespie, A. R., A. B. Kahle, and R. E. Walker, 1986, Color enhancement of highly correlated images. I. Decorrelation and HSI contrast stretches, Remote Sensing of Environment, Vol. 20, pp. 209-235.

McCauley, J. F., G. G. Schaber, C. S. Breed, M. J. Grolier, C. V. Haynes, B. Issawi, C. Elachi, and R. Blom, 1982, Subsurface valleys and geoarchaeology of the eastern Sahara revealed by Shuttle radar, Science, Vol. 218, pp. 1004-1020.

McClure, H. A., 1976, Radiocarbon chronology of late Quaternary lakes in the Arabian Desert, Nature, Vol. 263, pp. 755-756.

McClure, H. A., 1978, Ar Rub al Khali, (in) Quaternary Period in Saudi Arabia, Springer-Verlag, Wien, pp. 252-263.

Peake, W. H. and T. L. Oliver, 1971, The Response of Terrestrial Surfaces at Microwave Frequencies, Report APAL-TR-70-301, Ohio State University Electroscience Laboratory, Columbus, 255 p.

Powers, R. W., L. F. Ramirez, C. D. Redmond, and E. L. Elberg, Jr., 1966, Geology of the Arabian Peninsula, Sedimentary Geology of Saudi Arabia, USGS Prof. Paper 560-D, U. S. Govt. Printing Office, Washington, D. C., 147 p.

Roth, L. E. and C. Elachi, 1975, Coherent electromagnetic losses by scattering from volume inhomogeneities, IEEE Transactions on Antennas and Propagation, Vol. AP-23, pp. 674-675.

Schaber, G. G., J. F. McCauley, C. S. Breed, and G. R. Olhoeft, 1986, Shuttle Imaging Radar: Physical controls on signal penetration and subsurface scattering in the eastern Sahara, IEEE Transactions on Geoscience and Remote Sensing, Vol. GE-24, pp. 603-623.

Schaber, G. G., R. J. Pike, and G. L. Berlin, 1980, Terrain-analysis procedures for modeling radar backscatter, (in) Radar Geology: An Assessment, Jet Propulsion Laboratory, Pasadena, JPL Pub. 80-61, pp. 168-199.

UNESCO, 1977, Map of the World Distribution of Arid Regions and Explanatory Note, United Nations, Paris, 54 p. and 1:25 million-scale map.

Williams, P. L., D. Vaslet, P. R. Johnson, A. Berthiaux, P. Le Strat, and J. Fourniguet, 1986, Geologic Map of the Jabal Habashi Quadrangle, Sheet 26F, Kingdom of Saudi Arabia (with text), Geoscience Map GM-98C, Saudi Arabian Deputy Ministry for Mineral Resources, scale 1:250,000.

Zarins, J., 1986, MAR-TU and the land of Dilmun, (in) Bahrain Through the Ages - The Archaeology, KPI Limited, London, pp. 233-250.

Table 1. Grain-size analyses for collected sand samples.

Site	Gravel %	Sand %	Mean %	Median mm	Mean mm	Mode mm
Al Khunfah[a]						
1	0.0	99.5	0.5	0.35	0.29	0.35
2	0.0	98.8	1.2	0.25	0.35	0.49
Al Labbah[b]						
2	0.0	99.9	0.1	0.14	0.15	0.15
4	0.1	95.9	4.1	0.28	0.24	0.09
Harrat Hutaymah[c]						
3	2.8	94.3	2.9	0.51	0.43	0.71
4	3.7	93.3	3.0	0.65	0.29	0.35
6	1.0	98.0	1.0	0.37	0.38	0.35

[a]Sampling sites are shown in Figure 8.

[b]Sampling sites are shown in Figure 13 and 14.

[c]Sampling sites are shown in Figure 19.

Table 2. Microrelief and cover statistics for the Harrat Hautaymah study area.

Site[a]	Maximum Relief (cm)	Mean Relief (cm)	Sand Cover (%)
1	27.2	8.59	<5.0
2	22.5	8.04	<5.0
3	4.5	1.13	72.2
4	3.7	1.92	74.6
5	7.3	1.75	64.0
6	6.7	2.02	67.9
7	5.1	1.04	76.3

[a]Sampling sites are shown in Figure 19.

Table 3. Digitized SIR-A DN statistics for three surface units in the Harrat Hutaymah study area.[a]

Site[b]	Minimim DN	Maximum DN	Mean DN	S.D.
Exposed Lava				
1	162	211	187.6	14.7
2	135	204	179.2	16.2
Obscured Lava				
3	76	114	96.6	12.5
4	77	142	97.7	17.2
5	74	137	96.2	17.0
6	67	107	82.8	12.8
7	76	129	91.7	14.2
Eluvium				
8	53	61	56.0	2.3
9	54	65	57.7	2.8

[a]Windows measured 5 x 5 pixels.

[b]Sampling sites are shown in Figure 19.

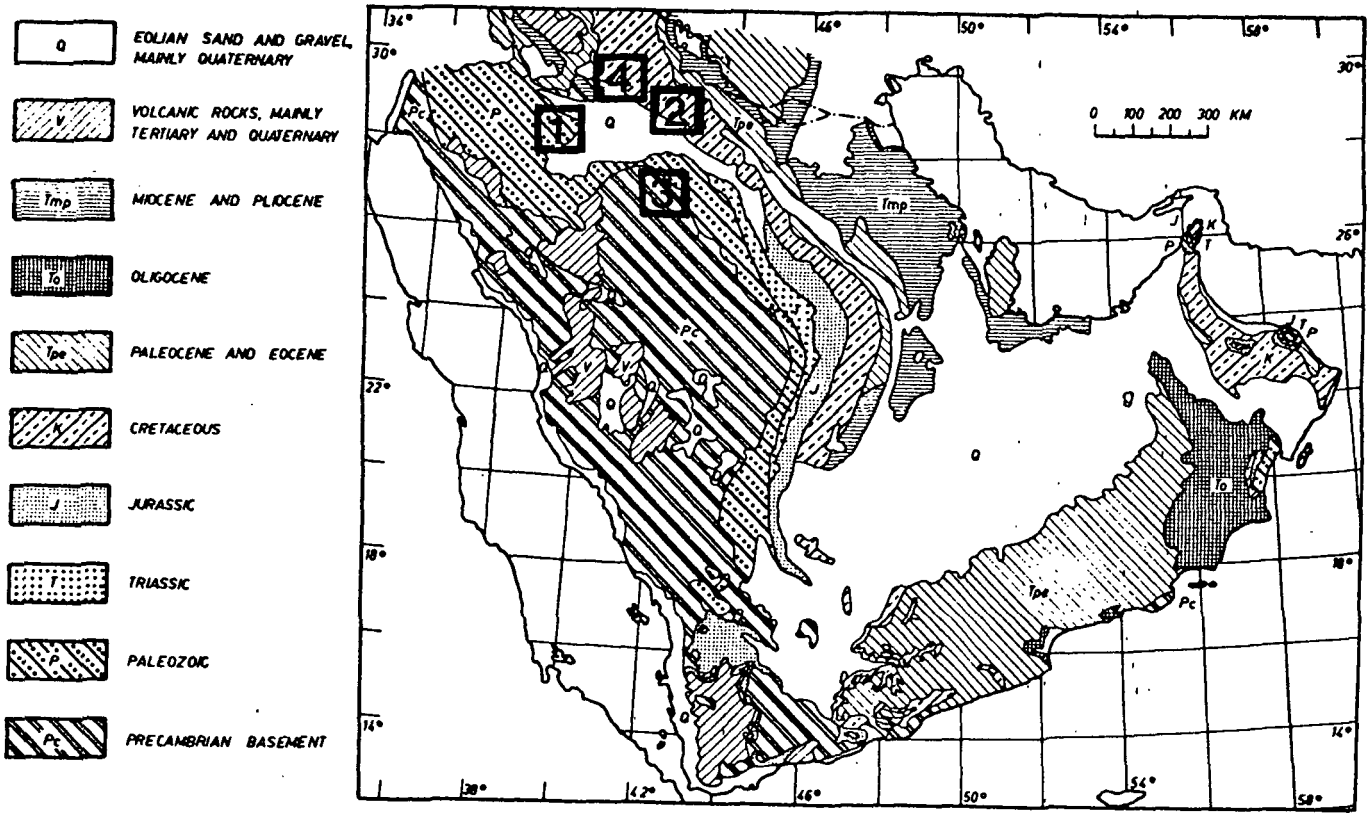

Figure 1. Generalized geology map of the Arabian Peninsula showing the locations of the three study sites addressed by this investigation. Sites 1 and 2 are located in the Arabian Shelf region. Site #3 is located in the Arabian Shield region. The three study sites have been blanketed with eolian sand of Quaternary age. Site #4 depicts the area where SIR-A and SIR-B subsurface imaging was earlier documented by Berlin et al. (1985, 1986).

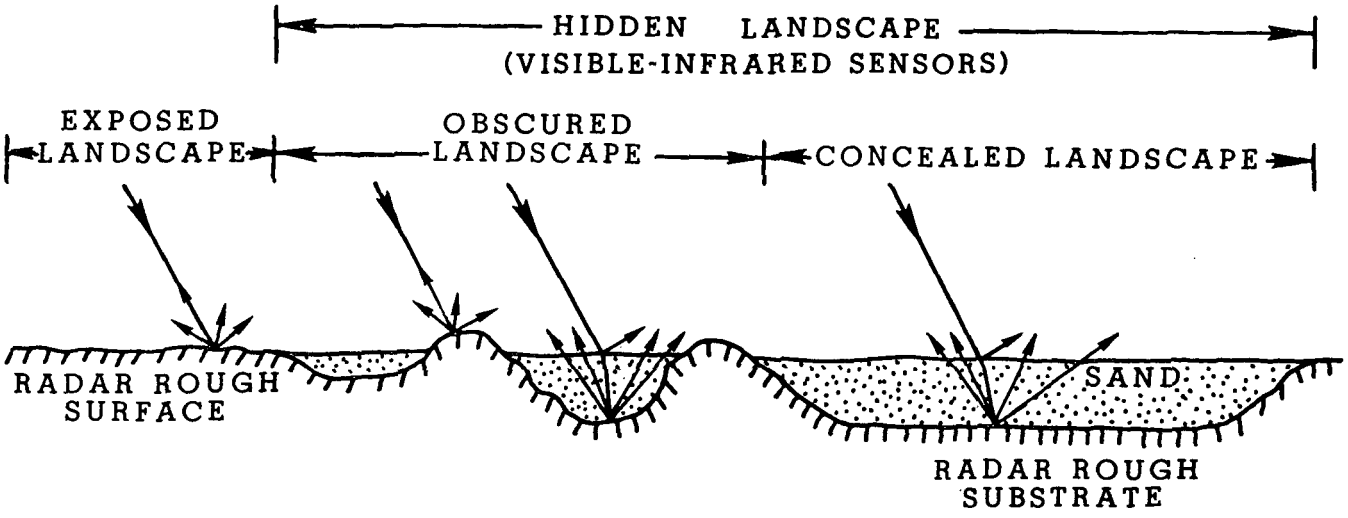

Figure 2. Diagram showing the two types of hidden landscapes that were detected by the SIR sensors in Saudi Arabia as indicated by the subsurface reflection profiles, but not by VIR sensors for the most part. Both SIR and VIR sensors can detect the exposed landscape. "Radar rough" pertains to the scale of a material's average vertical relief in relation to the wavelength and illumination geometry of the propagated radar energy that will cause diffuse reflection.

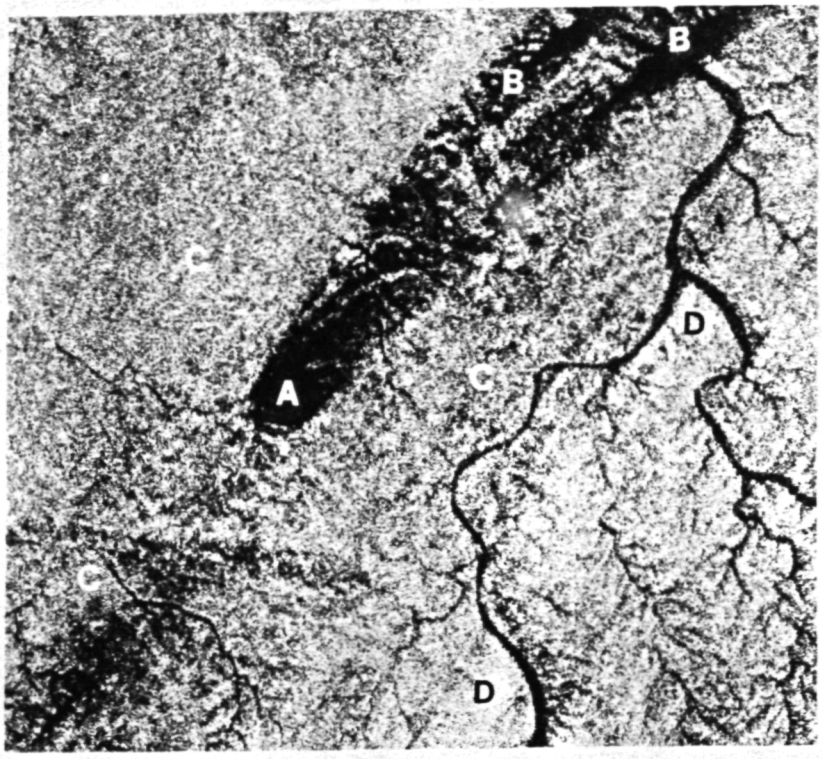

Figure 3. SIR-A L-band (23.5-cm wavelength) radar image of study area on the Al Labbah Plateau, acquired in November 1981. Look angle is about 47° and resolution is 40 m. Image scale is 1:250,000. Annotations are as follows: (A) a sand hill called Anbat, (B) a sand shadow (two wings) called Irq al Ubaytir, (C) the informally named Al Labbah sand sheet that was penetrated by both SIR-A and SIR-B beams, and (D) outcrop surface of the Upper Cretaceous Aruma Formation (primarily a shallow-water limestone). Note the similar tonal signatures for the surface and buried expressions of the Aruma Formation.

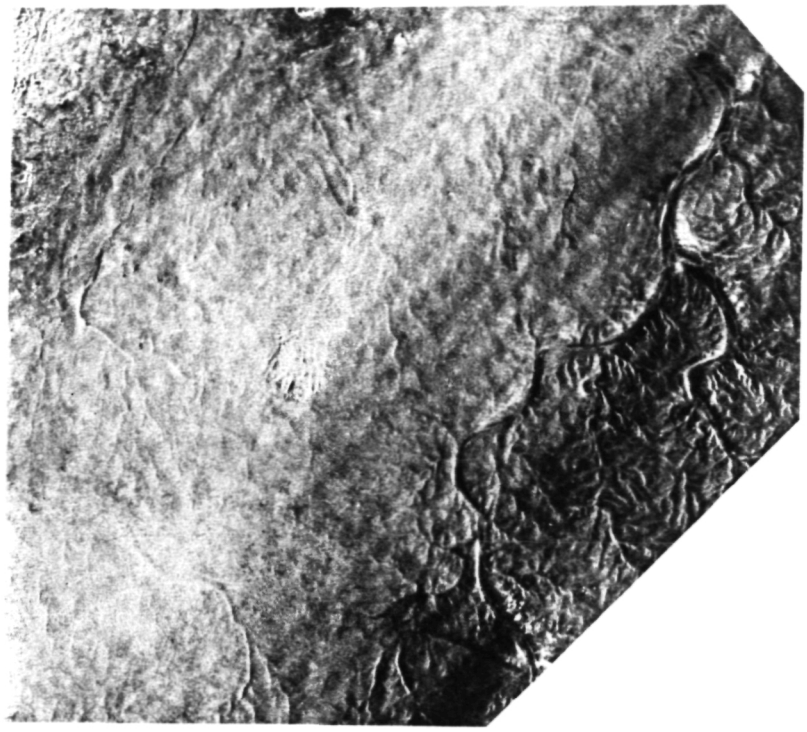

Figure 4. Landsat TM color-infrared image of study area on the Al Labbah Plateau, acquired on October 12, 1984. The band/color assignments are as follows: Band 2 = blue, Band 3 = green, and Band 4 = red. Each band incorporates a linear stretch to increase scene contrast while preserving original radiance relationships. Image scale is 1:250,000, and resolution is 30 m. Eolian sand cover is depicted in yellowish-red hues. Compare with Figure 3.

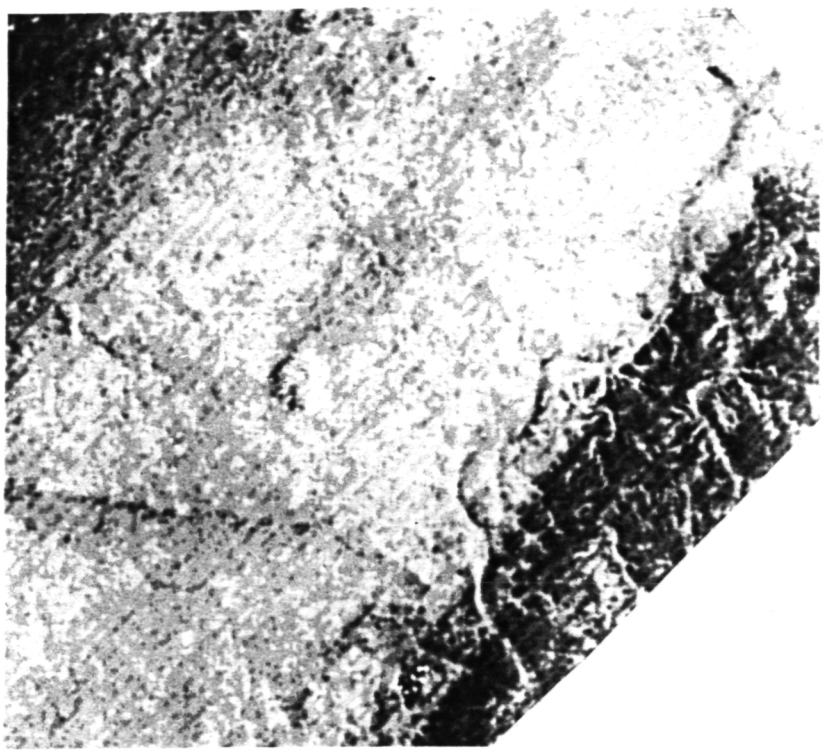

Figure 5. Landsat TM-6 thermal-infrared image of study area on the Al Labbah Plateau, acquired on October 12, 1984 at about 9:40 a.m. mean Sun time. The image incorporates a linear stretch to increase scene contrast while preserving original radiance relationships. Image scale is 1:250,000, and resolution is 120 m. Rock exposures contrast markedly with sand deposits because they have much higher thermal capacity and conductivity measures than the loosely packed sand; these parameters result in lower radiant temperatures for the rock exposures, and, hence, relative dark image tones. Compare with Figure 3.

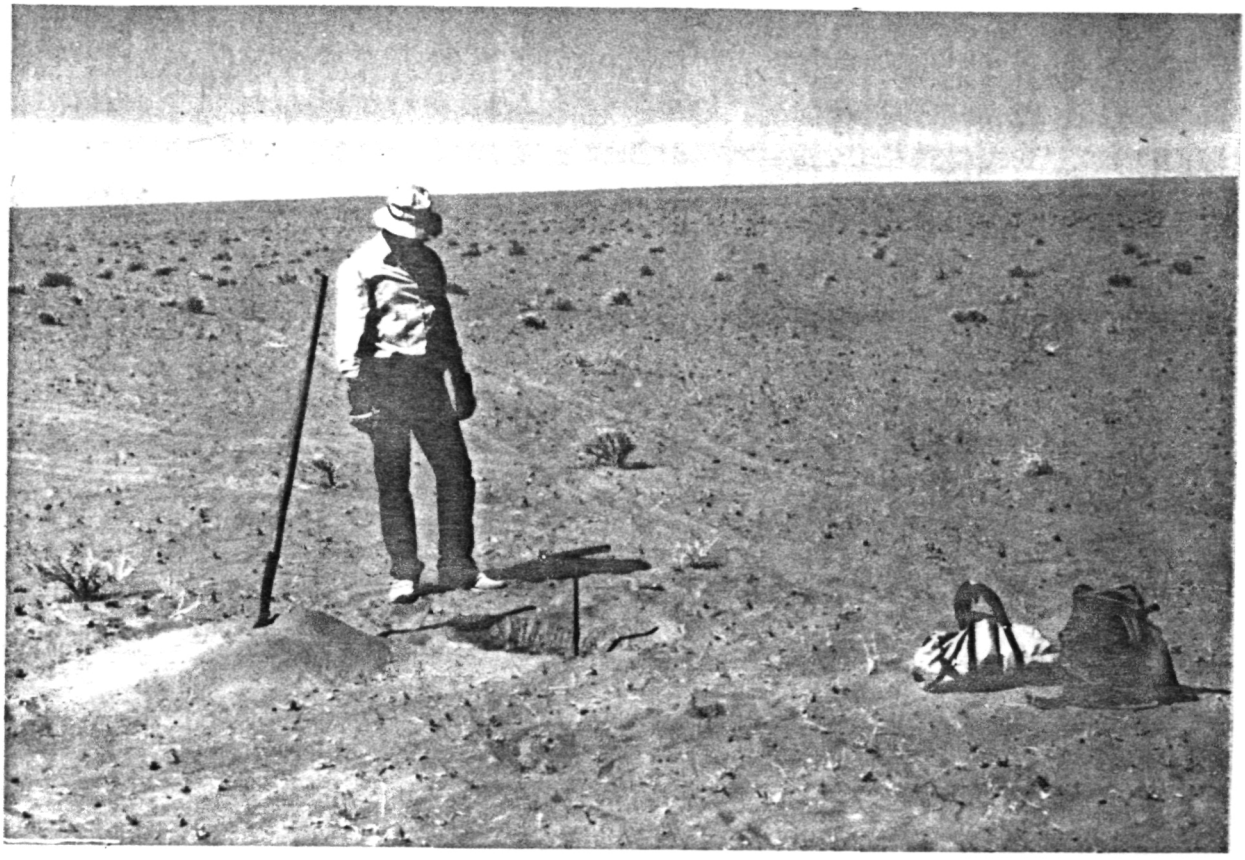

Figure 6. Ground view of the Al Labbah sand sheet that was penetrated by both SIR-A and SIR-B beams. Excavated pit is 82-cm deep. Xerophytic shrub cover (Haloxylon salicornicum) is less than 1 percent.

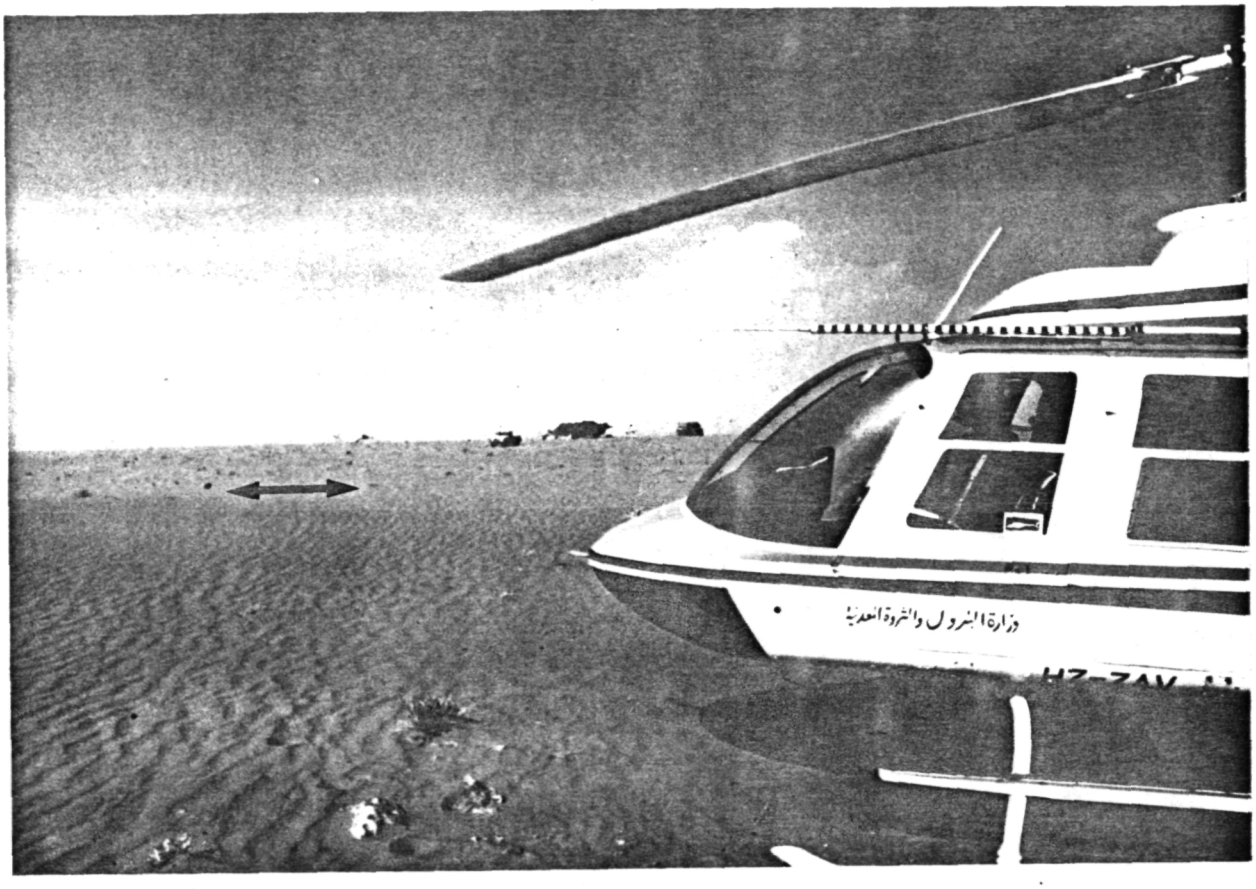

Figure 7. Ground view from the Al Labbah sand sheet north to the southern wing of the Irq al Ubaytir sand shadow. Approximate contact between the two eolian bedforms is at the double arrow. In this view, the thickness of the sand sheet is about 30 cm, while that for the sand shadow is about 3.1 m. Shown is a Bedowin camp on the local high ground.

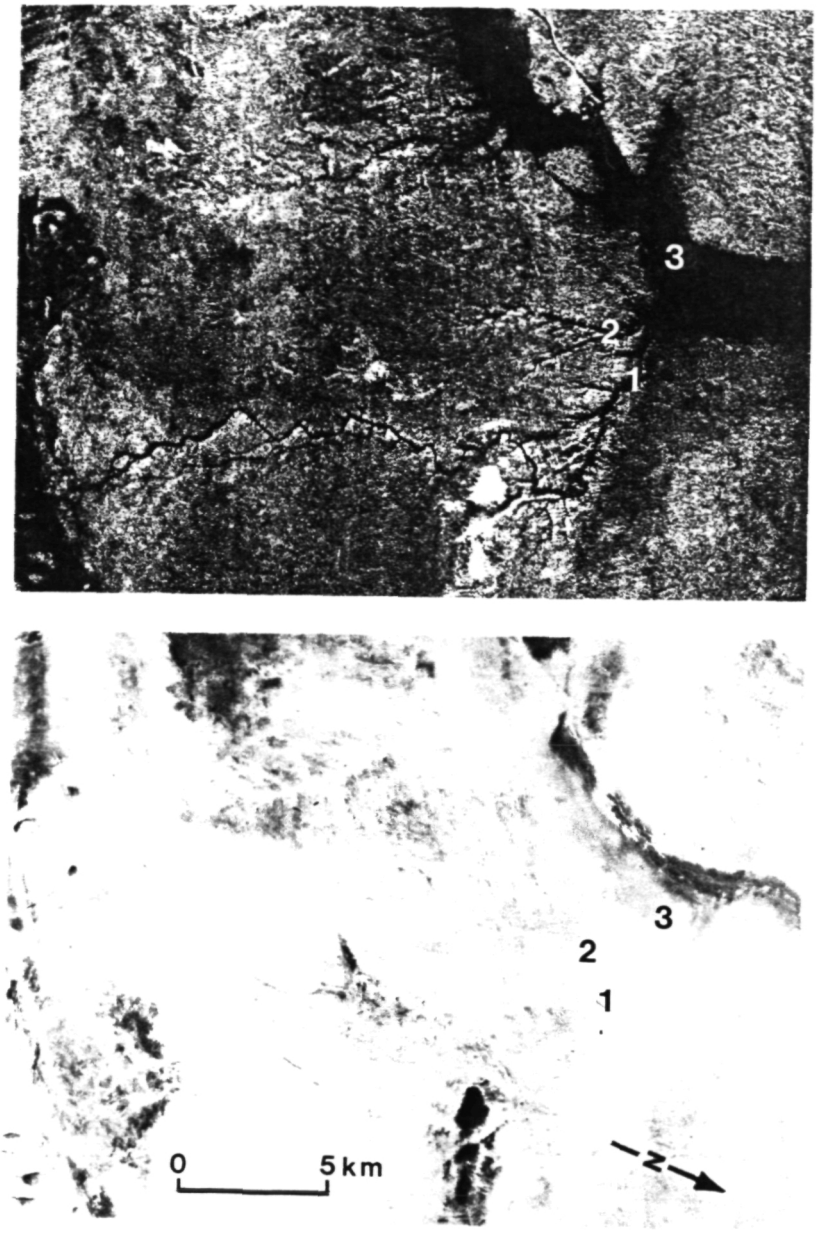

Figure 8. Multisensor view of the Al Khunfah Plateau and Wadi Nayyal paleodrainage system. At the top is the SIR-A L-band (23.3-cm wavelength) image that was acquired in November 1981. Look angle is 47° and resolution is 40 m. At the bottom is the LFC panchromatic photograph that was acquired during the SIR-B mission in October 1984; resolution is 15 m. Aerial views of locations 1-3 are presented in Figures 9-11.

Figure 9. Oblique aerial view showing a concealed or buried landscape at A and an obscured or partially buried landscape at B on the Al Khunfah Plateau (Site #1 in Figure 8). Sand cover at B is about 80 percent. Note that the tributary to Wadi Nayyal is nearly filled with eolian sand. Small barchanoid dunes in the foreground are transverse to the prevailing wind direction. Xerophytic shrub cover Haloxylon salicornicum) is less than 3 percent. View is to the east.

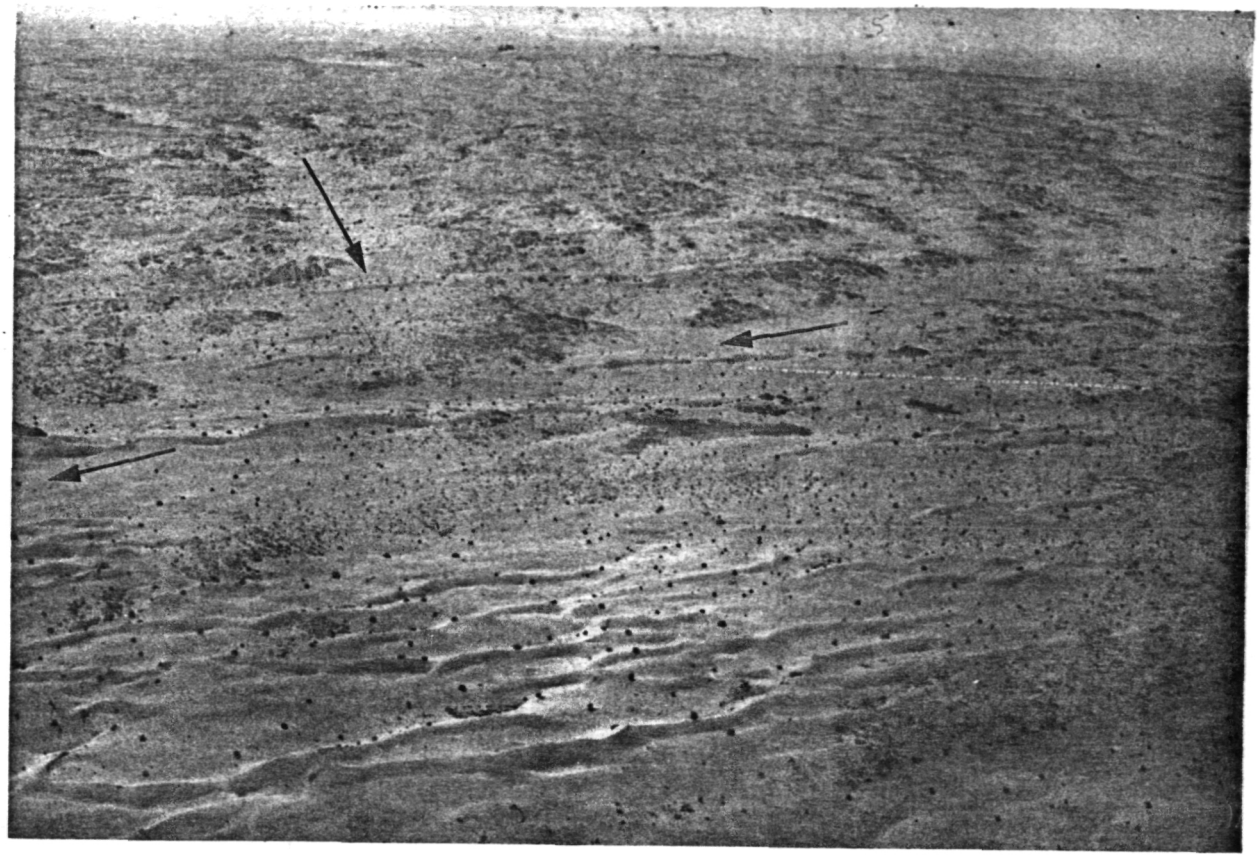

Figure 10. Oblique aerial view of drift sand covering much of the Tawil sandstone (obscured or partially buried landscape) and V-shaped paleowadi system that once was a tributary to Wadi Nayyal (Site #2 in Figure 8). Arrows mark the sand-filled wadi courses. Small barchanoid dunes in the foreground are transverse to the prevailing wind direction. Xerophytic shrub cover (Haloxylon salicornicum) is less than 3 percent. View is to the south.

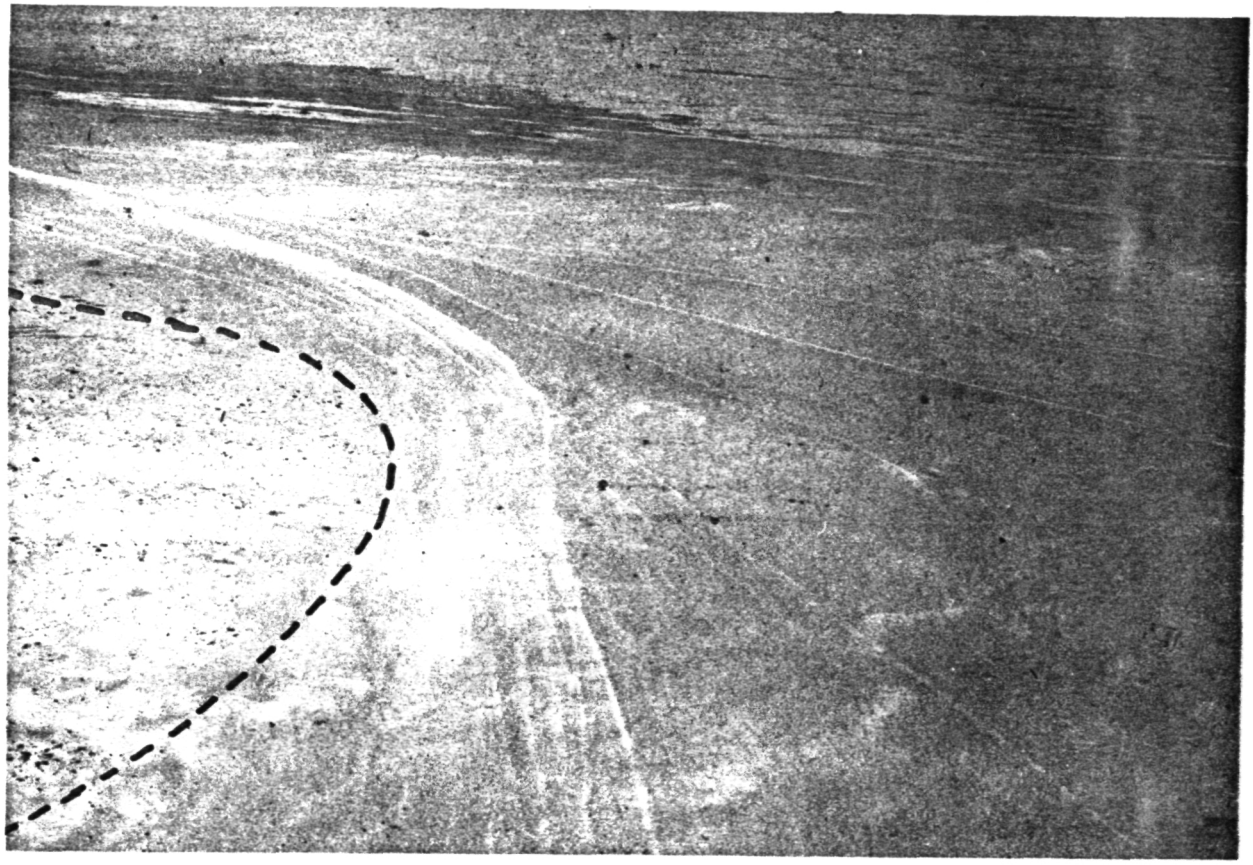

Figure 11. Oblique aerial view of the defunct Wadi Nayyal (Site #3 in Figure 8). Dashed line represents the approximate contact between the wadi floor and the sand veneered, upland surface. Dark areas on the wadi floor are Tertiary gravel deposits (largely ferruginous stained) that are not covered by eolian sand. Wadi Nayyal now serves as a transportation route for local Bedowin. View is to the north.

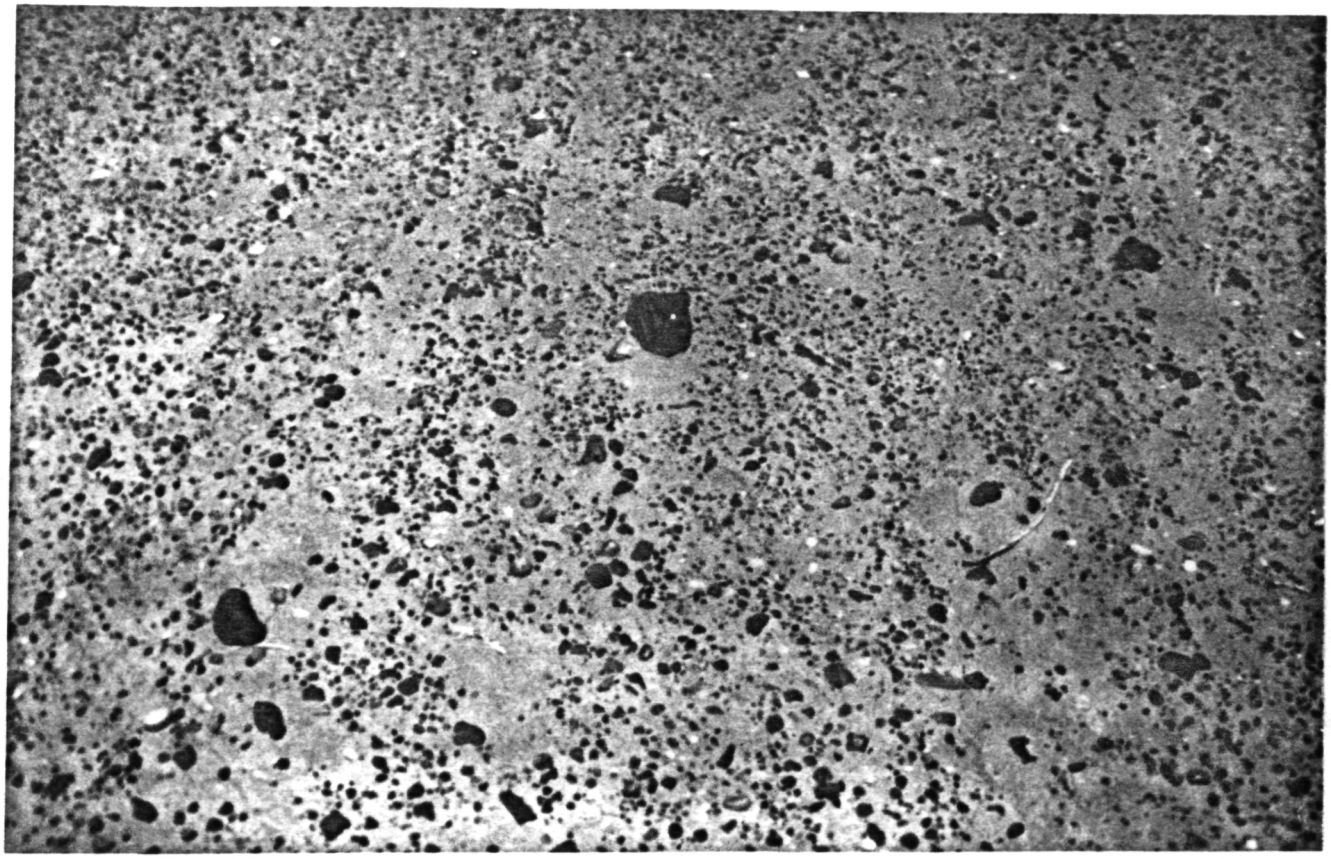

Figure 12. Close-up view of a typical surface of Wadi Nayyal. Most of the dark pebbles originated in the Arabian Shield--the wadi's original catchment area. The sand matrix is eolian. In this area of the wadi floor, mean surface roughness, measured over a 1.5-m templet baselength, equals 0.75 cm. Compass case measures 8.5x9.0 cm.

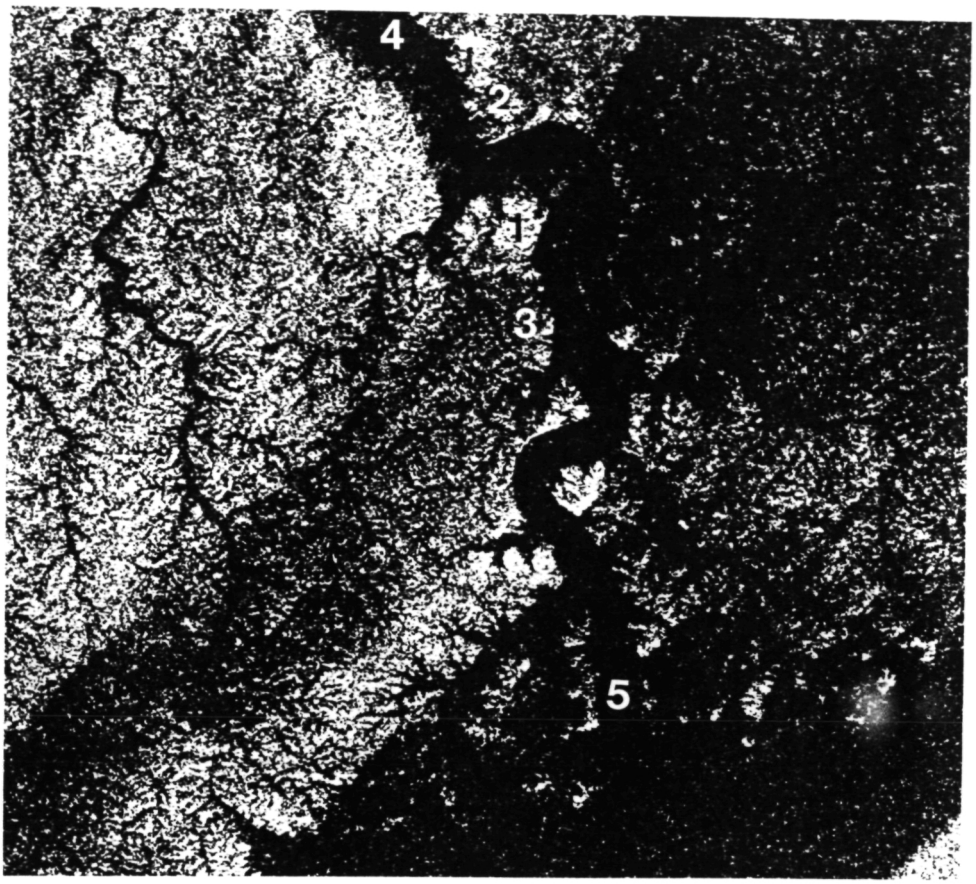

Figure 13. Computer-enhanced, SIR-B image of the Al Labbah and Wadi Al Khirr paleodrainage system. The L-band image was acquired in October 1984. Look angle is 36^{o}, and resolution is approximately 25 m. The digital image incorporates corrections for speckle and radiometric noise (Chavez and Berlin 1986) and a linear stretch to increase scene contrast while preserving original backscatter relationships. Image scale is 1:250,000. Numbers refer to ground sampling sites which are discussed in the text.

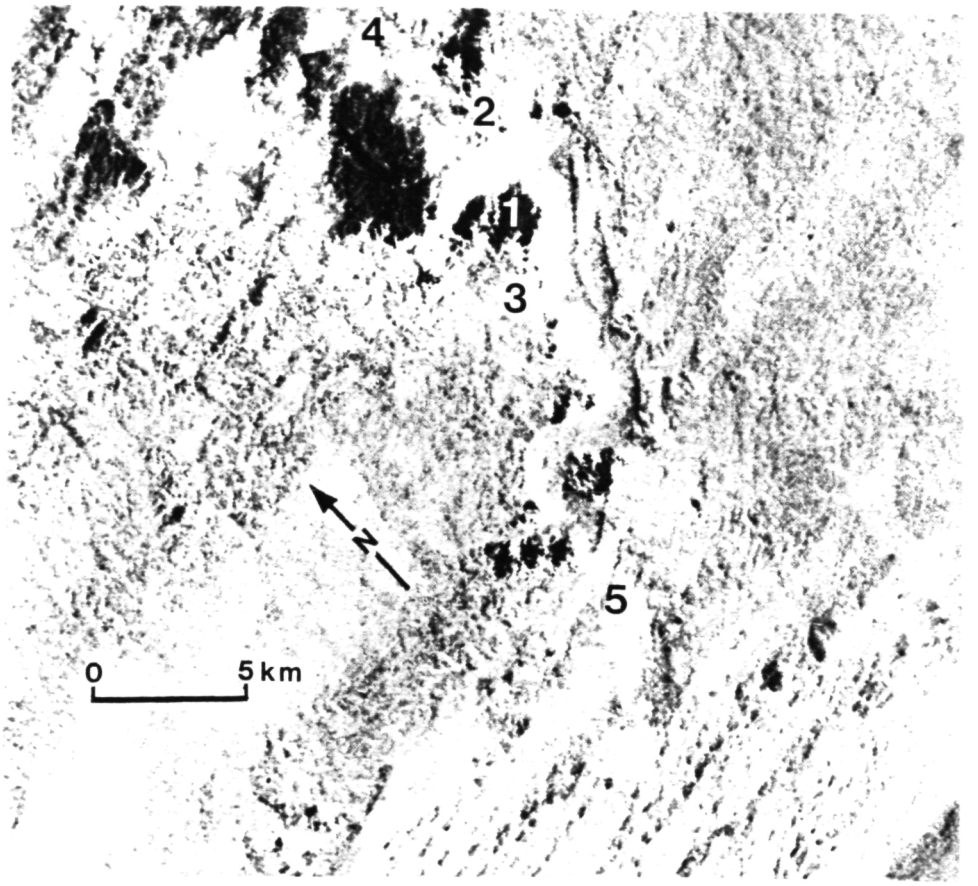

Figure 14. Computer-enhanced, Landsat MSS band 7 image of the Al Labbah Plateau and Wadi Al Khirr paleodrainage system. The image was acquired on June 2, 1973; resolution is approximately 80 m. The digital image was subjected to a high-pass filtering operation to enhance high-frequency spatial information (Avery and Berlin 1985) and a linear stretch to increase scene contrast while preserving original radiance relationships. Image scale is 1:250,000. Numbers refer to ground sampling sites which are discussed in the text. Compare with Figure 13.

Figure 15. Close-up view of a typical outcrop of the Aruma Formation (Site #1 in Figures 13 and 14). Mean surface roughness in this view, measured over a 1.4-m templet baselength, equals 10.7 cm. Consequently, this type of rubbly surface is radar rough or Lambertian at L-band wavelengths. Notebook measures 14x22.5 cm.

Figure 16. Close-up view of drift sand covering much of the Aruma Formation s surface rubble (Site #2 in Figures 13 and 14). Effective surface roghness of Aruma blocks is diminished because of the presence of eolian "fill" sand. Mean surface roughness in this area, measured over a 1.5-m templet baselength, equals 4.2 cm. Sand cover is about 65 percent. Pen is 13.5-cm long.

Figure 17. Close-up view of drift sand covering much of the Aruma Formation's surface rubble (Site #3 in Figures 13 and 14). Effective surface roughness of Aruma blocks is diminished because of the presence of eolian "fill" sand. Sand cover is about 72 percent. Pen is 13.5-cm long.

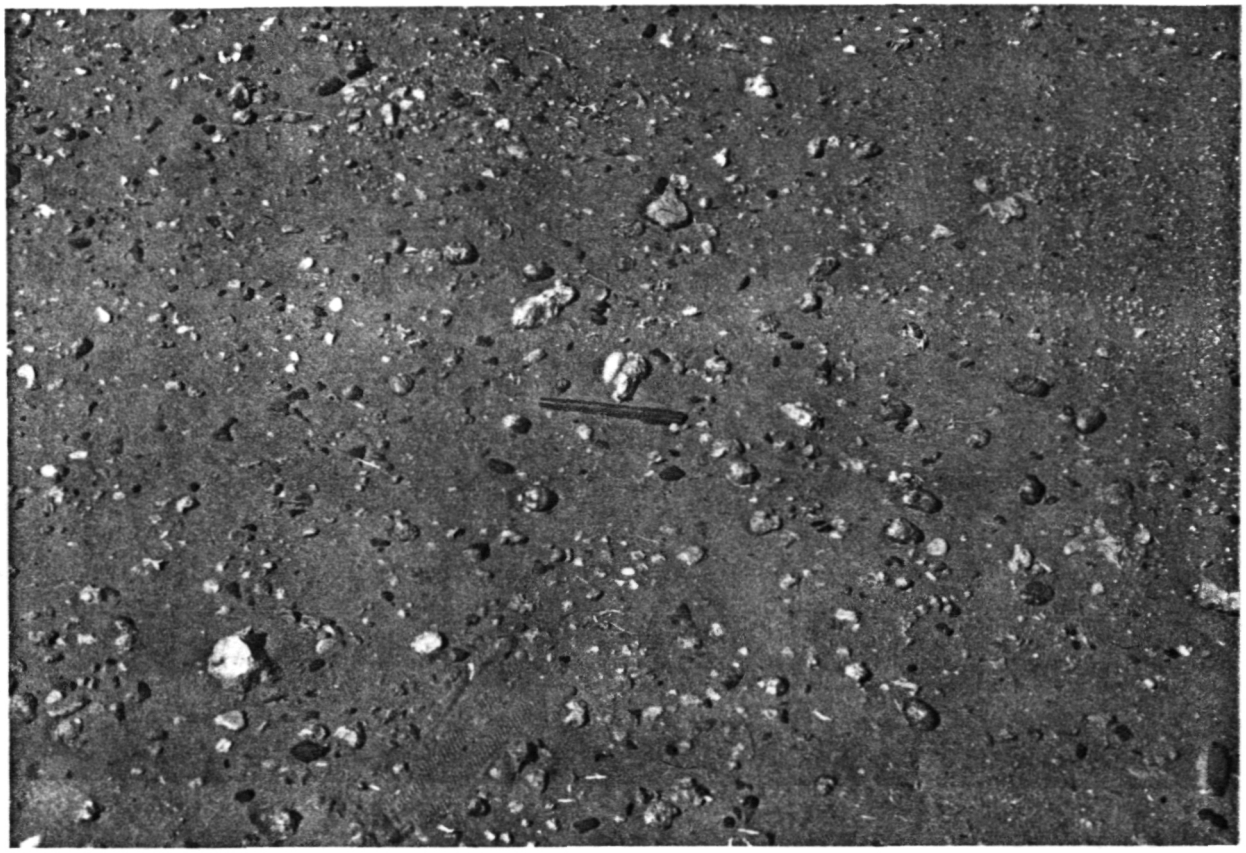

Figure 18. Close-up view of a typical surface of Wadi Al Khirr (Site #4 in Figures 13 and 14). Most of the angular pebbles (limestone, dolomite) are from the local Aruma Formation. The stream rounded pebbles (quartzite, granite, rhyolite, basalt) are from the distant Arabian Shield. In this area of the wadi floor, mean surface roughness, measured over a 1.5-m templet baselength, equals 0.82 cm. Pen is 13.5-cm long.

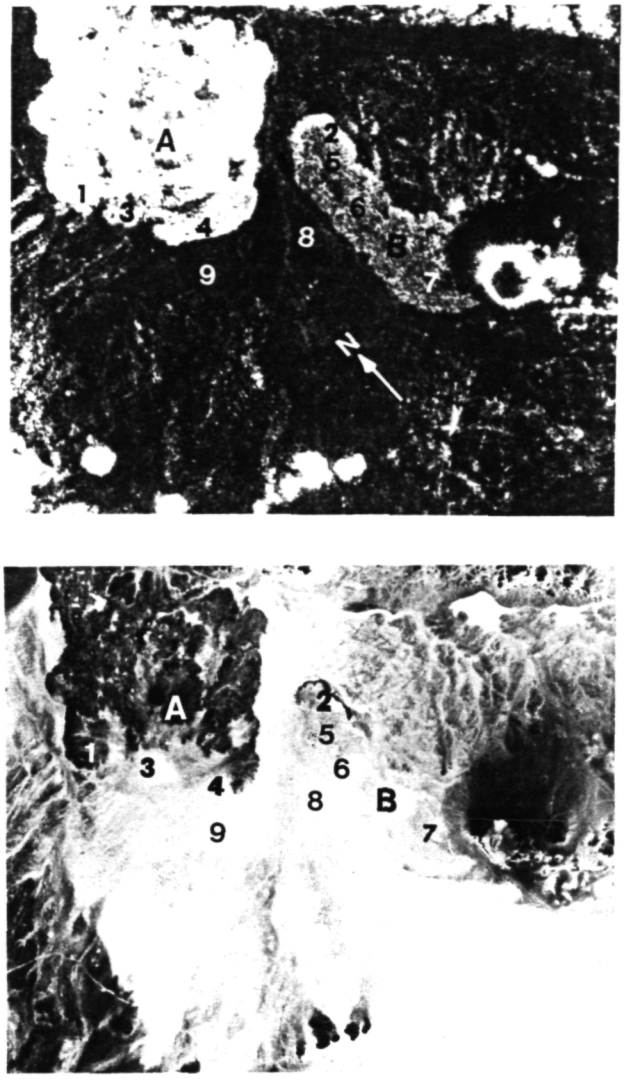

Figure 19. Multisensor view of the Harrat Hutaymah study area. At top is the SIR-A image that was acquired in November 1981. Look angle is about 47°, and resolution is 40 m. At the bottom is the Landsat TM color-infrared image that was acquired on August 18, 1984 with a sun angle of 58°. The band/color assignments are as follows: Band 2 = blue, Band 3 = green, and Band 4 = red. Resolution is 30 m. Both images are printed at a scale of 1:250,000. Of primary interest to this investigation are two lava flows: A = Najafat Umm Harruj and B = Ath Thu'aylibi. Numbers refer to ground sampling sites which are described in the text.

Figure 20. Overview of exposed aa surface on the Najafat Umm Harruj lava flow (Site #1 in Figure 19). Based upon Fisher's (1961) classification, most of the pyroclastic fragments in this view are blocks (greater than 64 mm in diameter). Sand cover is less than 5 percent, and mean surface roughness, measured over a 1.5-m templet baselength, is 8.59 cm (Table 2). Backpack measures 30x50 cm.

Figure 21. Overview of exposed aa surface at the distal end of the Ath Thu'aylibi lava flow (Site #2 in Figure 19). Based upon Fisher's classification, most of the pyroclastic fragments in this view are blocks (greater than 64 mm in diameter). Sand cover is less than 5 percent, and mean surface roughness, measured over a 1.5-m templet baselength, is 8.04 cm (Table 2).

Figure 22. Close-up view of sand-obscured surface of the Najafat Umm Harruj lava flow (Site #3 in Figure 19). Effective surface roughness of pyroclastic fragments is diminished because of the presence of eolian "fill" sand. Sand cover is about 72 percent, and mean surface roughness, measured over a 1.5-m templet baselength, is 1.13 cm (Table 2). Backpack measures 30x50 cm.

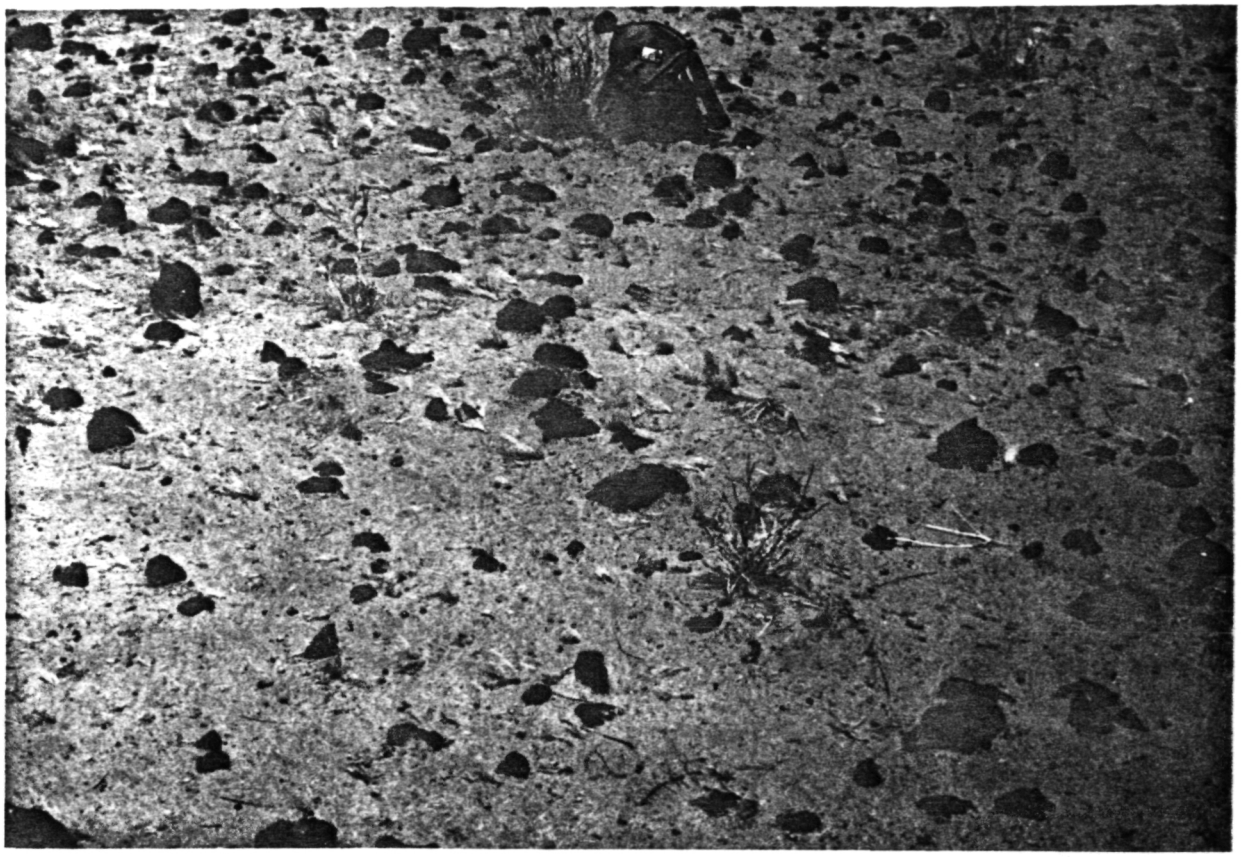

Figure 23. Close-up view of sand-obscured surface of the Ath Thu'aylibi lava flow (Site #7 in Figure 19). Effective surface roughness of pyroclastic fragments is diminished because of the presence of eolian "fill" sand. Sand cover is about 76 percent, and mean surface roughness, measured over a 1.5-m templet baselength, is 1.04 cm (Table 2). Backpack measures 30x50 cm.

Figure 24. Oblique aerial view of the western portion of the Najafat Umm Harruj lava flow, showing exposed (Site #1) and sand-veneered (Sites 3 and 4) flow surfaces. View is to the northwest. See Figures 19-20, 22 and Table 2.

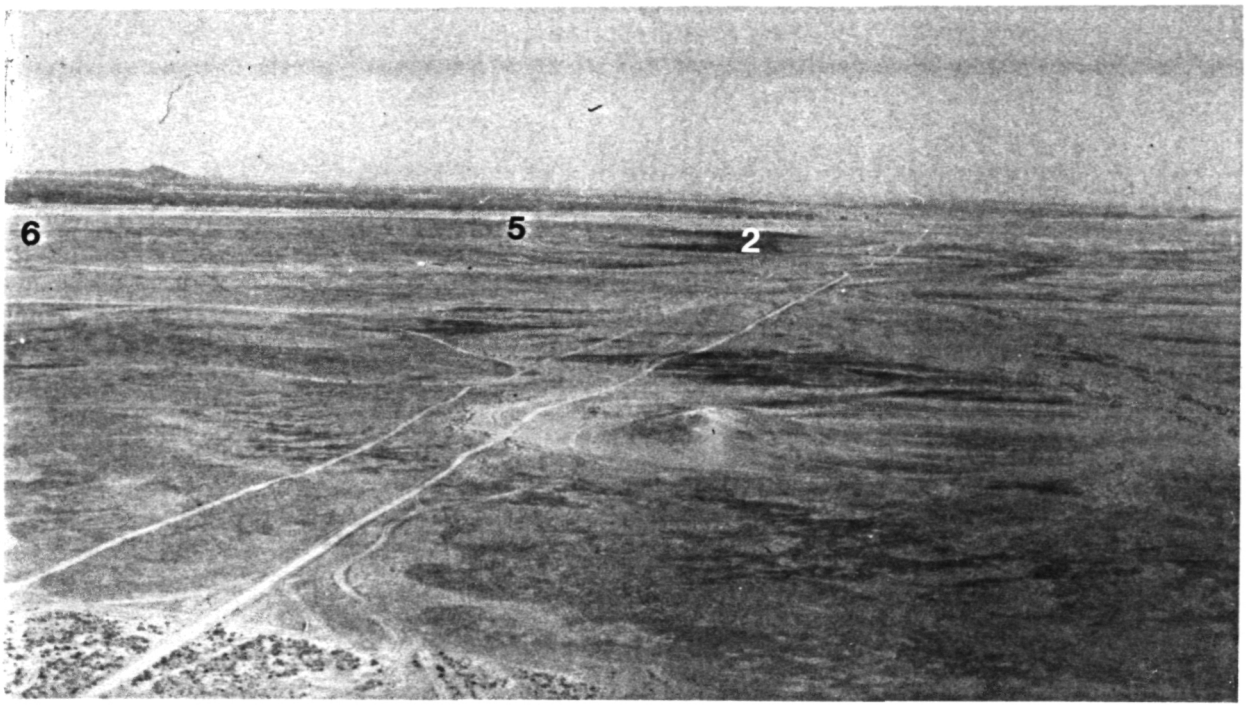

Figure 25. Oblique aerial view of the eastern portion of the Ath Thu'aylibi lava flow, showing exposed (Site #2) and sand-veneered (Sites 5 and 6) flow surfaces. Note that the flow margin is not detectable to the left of Site #2. View is to the west. See Figures 19 and 21 and Table 2.

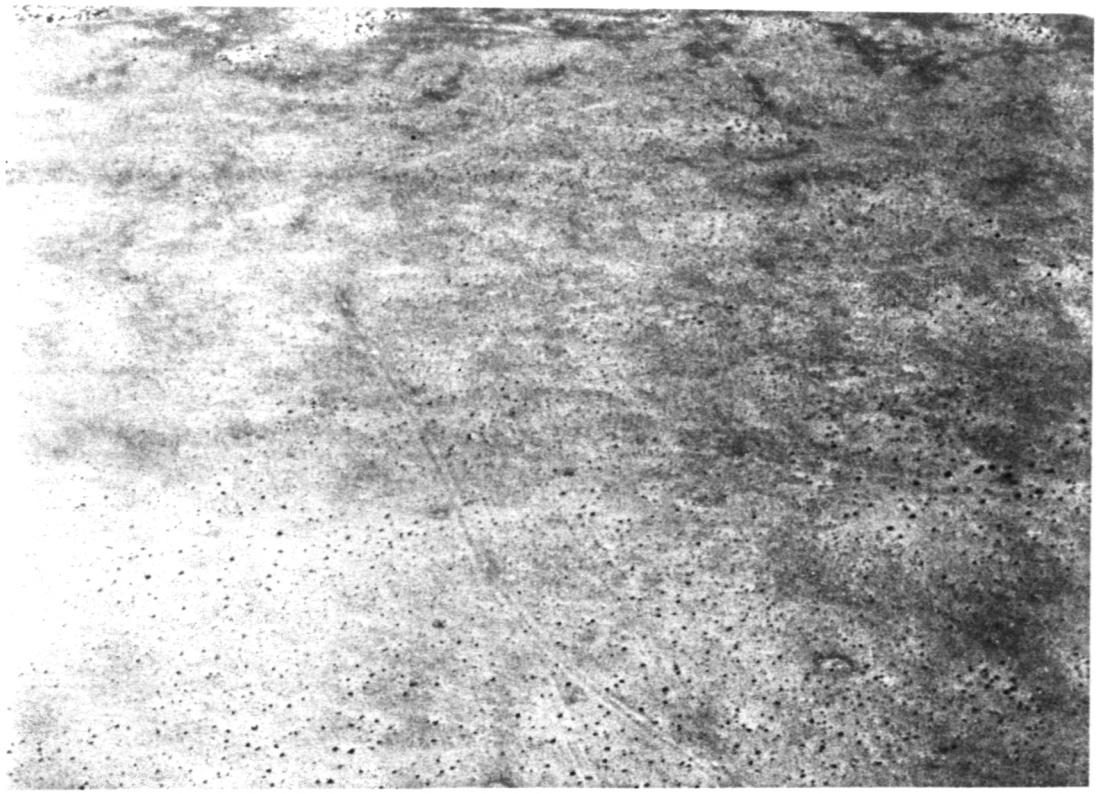

Figure 26. Oblique aerial view of the sand-veneered surface of the Ath Thu'aylibi lava flow. View includes ground-sampling Site #6 (Figure 19 and Table 2). Note vehicle tracks made by local Bedowin herdsmen.

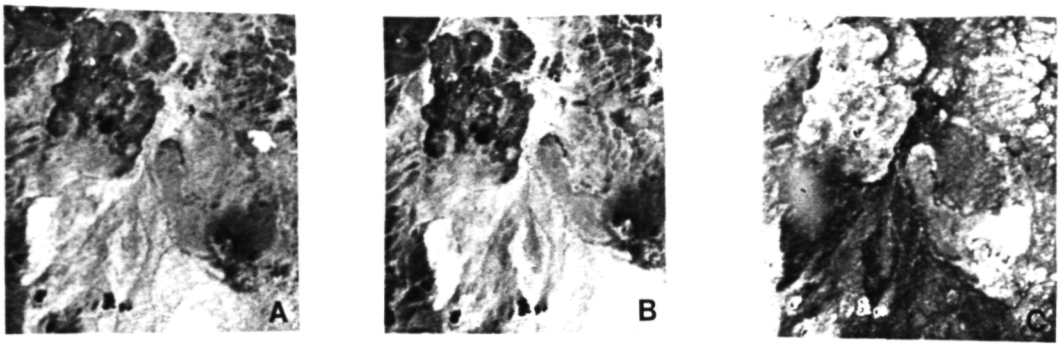

Figure 27. Computer-processed, Landsat MSS color-composite images of the Harrat Uutaymah study area: (A) = simulated natural-color image (Eliason et al. 1974): Band "3" = blue, Band 4 = green, Band 5 = red; (B) = color-infrared image, incorporating linear contrast stretches: Band 4 = blue, Band 5 = green, Band 7 = red; and (C) = false-color image, incorporating sinusoidal contrast stretches (Avery and Berlin 1985): Band 4 = blue, Band 5 = green, Band 7 = red. The MSS data were acquired on November 20, 1972. Image scale is 1:500,000. Compare with Figure 19.

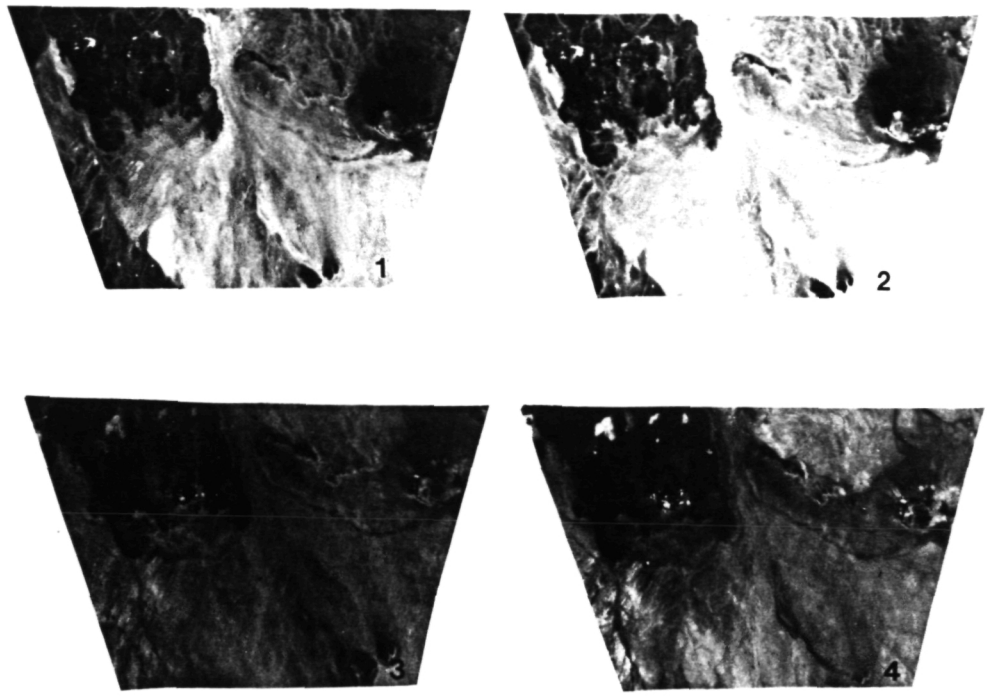

Figure 28. Computer-processed, Landsat TM color-composite images of the Harrat Hutaymah study area: (1) = natural-color image: Band 1 = blue, Band 2 = green, Band 3 = red; (2) = false-color image: Band 1 = blue, Band 4 = green, Band 7 = red; (3) = band-ratio image: Bands 4/1 = blue, Bands 5/4 = green, Bands 7/5 = red; and (4) = principal-component image of TM Bands 1, 4, and 7: PC-1 = blue, PC-2 = green, PC-3 = red. The images are printed at a scale of 1:500,000. Compare with Figure 19.

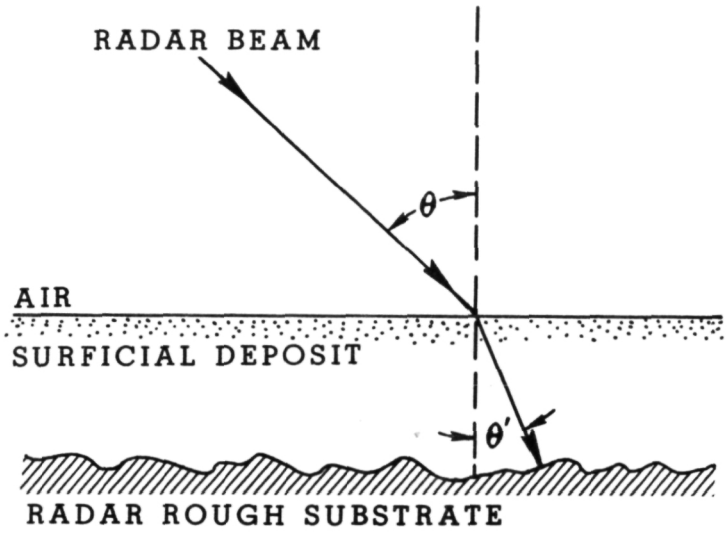

Figure 29. Diagram illustrating refraction of the propagated radar beam at the air-sand interface.

Figure 30. Oblique aerial view of a MAR-TU animal trap that was used for the killing of orax, gazelle, wild goat, onager, and ostrich (all now extinct in Saudi Arabia). The animals were stampeded down the guiding arms, through the neck, and into the enclosure. The circular hides concealed archers and spearmen.

DETECTION OF HIDDEN LANDSCAPES IN SAUDI ARABIA WITH SHUTTLE RADAR IMAGES

Graydon Lennis Berlin

Geography Department - Box 15016
Northern Arizona University
Flagstaff, Arizona 86011 USA

Mohammed A. Tarabzouni
Kamel M. Sheikho
Abdullah H. Al-Naser
King Abdulaziz City for Science and Technology
P.O. Box 6086
Riyadh 11442, Saudi Arabia

Accepted
Submitted for Publication in

American Institute of Aeronautics and Astronautics Journal

ABSTRACT

L-band radar images from the two NASA Shuttle Imaging Radar missions in 1981 and 1984 delineate and characterize a number of geologic terrains in Saudi Arabia that are completely or partially buried beneath relatively thin deposits of eolian sand. The sand mantle was essentially transparent because the propagated radar beams were able to penetrate through the fine-grained, loose, and very dry sand deposits and be diffusely reflected from various radar-rough substrates. These buried geologic terrains and landscapes were not amenable to detection by visible and infrared wavelength sensors because they recorded reflected and emitted energies coming from overburden. Our findings indicate that these unique radar views can provide valuable information for geologic, hydrologic, and archaeologic studies, and will be fully realized when country-wide, L-band radar image coverage is provided by the NASA Earth Observing System.

INTRODUCTION

Since 1982, we have been evaluating the utility of L-band radar images from the first and second NASA Shuttle Imaging Radar missions (SIR-A and SIR-B) for potential geologic, hydrologic, and archaeologic applications in Saudi Arabia. Images from eight data takes have been evaluated to date, and the most far reaching discovery has centered on the subsurface imaging capability of the SIR sensors [1,2]. Subsurface imaging represents a process whereby propagated SIR beams penetrated through relatively thin and very dry mantles of eolian sand and were diffusely reflected from a radar-rough substrate. Because a portion of the reflected pulses escaped the overburden and were detected by the antenna, the radar imaging system in essence made invisible or transparent the younger sand deposits and revealed older geologic terrains or hidden landscapes. Such older terrains were not amenable to detection by visible and infrared (VIR) wavelength sensors because of the masking effect of the overlying eolian sand deposits.

The purpose of this paper is to provide an overview discussion of the two major types of hidden landscapes that have been discovered in Saudia Arabia and the favorable ground conditions that, in conjunction with certain SIR system characteristics, explain radar backscatter or echo intensities for the hidden landscapes. Important SIR-A and SIR-B characteristics are presented in Table 1. Summaries of the SIR program and radar image interpretation principles are available in Avery and Berlin [3] and Sabins [4].

BACKGROUND

Saudi Arabia is well suited for subsurface radar imaging because many of its pre-Quaternary geologic terrains are mantled by extensive eolian sand deposits that are normally dry. The eolian veneer is largely the product of two arid phases in the Quaternary Period, including the last 6,000 years or so, when all of Saudi Arabia, except the mountainous southwestern region, has been dominated by eolian erosional and depositional processes. In northern Saudi Arabia, extensive areas of the Arabian Shelf's low-rolling sedimentary terrain have been accumulation zones for eolian sand originating from the An Nafud and Ad Dahna sand seas and from broad areas of poorly consolidated Paleozoic sandstones that are exposed in northwestern Saudi Arabia. In addition, large areas of the Red Sea Coastal Plain and Arabian Shield are veneered by thin, windblown sand deposits. Representative types of eolian cover include sand sheets or blankets, sand drifts, sand shadows, small dune fields, and paleowadi fill-sand.

These areas lie in arid and hyperarid bioclimatic zones that are characterized by precipitation/potential evapotranspiration ratios (P/Etp) of 0.03 to 0.2 and less than 0.03, respectively [5]. Mean annual precipitation is less than 120 mm. Rainfall, although unpredictable and irregular, occurs predominantly during the months between December and March. This winter maxima is extremely important because the SIR-A and SIR-B missions occurred in late fall, a time when the moisture content of the sand deposits would be at minimum levels. Because of the sparcity of rainfall, natural vegetation is restricted to scattered xerophytic shrubs and seasonal grasses.

SIR DETECTION OF HIDDEN LANDSCAPES

In areas of SIR-A and SIR-B signal penetration, ground surveys have identified two states of surficial material masking. In one case, the older geologic terrain is invisible over large areas because of its complete burial by windblown sand deposits; this condition produces what we call a concealed or buried landscape (Figure 1). For the second case, the geologic terrain is identifiable by direct field observation because sporadic outcrops can be seen protruding through the sand cover; this degree of masking is responsible for producing an obscured or partially buried landscape (Figure 1). Both total and partial masking can produce opaque or "blind" conditions for VIR sensors because of their inability to detect the subsurface. The term hidden landscape has been coined to encompass both the concealed and obscured states of terrain burial (Figure 1).

Because of SIR's subsurface imaging capability, the eolian cover is rendered essentially transparent under the correct conditions. Thus, in contrast to the VIR sensors, the SIR systems are capable of detecting both types of hidden landscapes (Figure 1). Both SIR and VIR sensor systems can detect exposed landscapes (Figure 1).

From a remote sensing perspective, concealed or buried geologic terrains cannot be detected by VIR sensors because they provide information about the reflectance and emittance properties of the surface material, in this case those of the overburden. Based upon field measurements, it has been determined that a partially buried geologic terrain (i.e., obscured landscape) can assume the characteristics of a buried landscape for VIR sensors when the amount of surficial material cover exceeds about 60 percent of the ground resolution cell. In this state, the VIR return signal is essentially determined by the reflectance and emittance properties of the surficial material. SIR backscatter or echo intensity, by comparison, is determined by both the surface and subsurface components of the radar-rough, geologic terrain unit, with no measurable input from the surficial overburden (Figure 1).

Hidden landscape features that have been identified on SIR imagery of Saudi Arabia include lava flow lobes, marine terrace deposits, bedrock contacts, and a number of paleodrainage details, including the lateral boundaries of master wadi valleys and bedrock-incised tributary networks. VIR data that have been used in comparative assessments are as follows: (1) computer-enhanced Landsat Multispectral (MSS) images (resolution = 80m); (2) computer-enhanced Landsat Thematic Mapper (TM) images (resolution = 30m and 120m); (3) Large Format Camera (LFC) panchromatic photographs (resolution = 15m). The following case histories have been selected to illustrate the unique ability of SIR to detect concealed and obscured landscapes.

The most dramatic example of SIR-A and SIR-B subsurface imaging of a buried or concealed landscape is along the southern margin of the Al Labbah Plateau (center coordinates: 29°35'N, 41°50'E), an aggradational adjacency to the An Nafud sand sea [1,2]. SIR-A and TM images of the study area are presented in Figure 2. The region is underlain by flat-lying rocks of the Upper Cretaceous Aruma Formation, which is primarily a shallow-water limestone. The outcrop surface of the Aruma Formation is commonly mantled with angular to subangular limestone rocks that vary in size from pebbles to cobbles, with varying concentrations of boulders (Figure 3). The local area is dominated by three eolian sand features: (1) a 37-m high sand hill called Anbat, (2) an elongated sand shadow (two wings) called Irq al Ubaytir, and (3) the informally named Al Labbah sand sheet (Figure 2).

Both the SIR-A and SIR-B beams penetrated through the widespread sand sheet and were diffusely reflected from the buried Aruma Formation. A surface view of the penetrated sand sheet is shown in Figure 4. Pits excavated in the sand sheet, revealed the presence of Aruma fragments similar in size to those where the Aruma is exposed (Figure 3). Both the surface and subsurface fragments were radar rough and thus responsible for scattering the incident radar beam in many directions, but with a sizable component being returned to the SIR antenna. Depth measurements from more than 80

test holes excavated in the sand sheet show that subsurface imaging occurred through a sand layer whose maximum measured thickness is 1.24 m.

Both the buried and surface exposures of the Aruma Formation are depicted as a bright tone in the SIR-A image (Figure 2). This phenomenon has been examined by Blom [6], who notes that there is usually insufficient information in a single radar image to determine whether the radar is detecting surface or subsurface terrain, and that VIR photographs or images are needed because they detect only surface exposures. This type of complementary analysis is illustrated by a comparison of the tonal signatures for hidden and exposed Aruma landscapes in the SIR-A and TM images (Figure 2).

Within the areal bounds of the penetrated sand sheet, the SIR-A image dramatically defines the thick sand deposits at Anbat and Irq al Ubaytir (Figure 2). These features are depicted as a dark tone in the SIR image because the radar signal was either unable to penetrate through their thicker sand layers to the reflecting substrate, or to exit the sand layer after subsurface reflection (Figure 2). The minimum thickness where subsurface imaging did not occur is estimated to be about 3.1 m; this occurred along the southern wing of Irq al Ubaytir (Figure 5).

The ability of SIR to detect a partially buried landscape is dramatically illustrated at the Al Khunfah Plateau study area (center coordinates: 28°30'N, 39°30'E). A SIR-A image and LFC photograph of the local region are presented in Figure 6. The Al Khunfah Plateau is an undulating plain that is underlain by the virtually flat-lying Tawil sandstone of Devonian age. The Tawil is a coarse, crossbedded sandstone that weathers to a rough, rubbly surface. Outcrops are normally coated with black desert varnish. The upland surface is now mostly covered by various thicknesses of loose drift sand, punctuated with local barchanoid dunes (Figures 7 and 8).

A feature of special interest is the aggraded Wadi Nayyal paleodrainage system (master stream valley and tributaries from local drainage basins) that was carved in bedrock by intensive runoff that occurred during late Tertiary and early Quaternary

pluvials. The dry wadi beds are surfaced with one or more of the following types of deposits: (1) late Tertiary stream-rounded and ferruginous stained gravel; (2) locally-derived Quaternary alluvium consisting of unconsolidated silt, sand, and gravel; and (3) eolian wadi-fill sand of Quaternary age. The latter type of deposit is especially common because many of the defunct wadi channels have acted as efficient sand traps throughout the late Quaternary because of their negative topographic expression and their transverse orientation to the prevailing wind direction (Figure 8).

Comparison of the SIR-A image and LFC photograph indicates that each portrays a dramatically different view of the study area (Figure 6). The LFC photo shows a contemporary terrain dominated by eolian sand deposits, while the SIR-A image reveals a predominantly paleo-fluvial terrain. The paleo-fluvial terrain is clearly defined in the SIR-A image because (1) varying thicknesses of drift sand overlying the Tawil sandstone of the remnant interfluves were penetrated by the propagated beam (bright image tone), and (2) the wadi beds were responsible for a minimal backscatter component (dark image tone) because the incident beam was largely reflected from their radar-smooth surfaces in a mirror-like fashion (i.e., away from the antenna) and/or attenuated in the channel fill. The LFC photograph shows little tonal contrast between the remnant interfluves and wadi beds because their sand veneered surfaces did not produce distinctive signatures at visible wavelengths.

GROUND CONDITIONS FAVORING SUBSURFACE IMAGING

Several favorable ground conditions, working simultaneously and in conjunction with desirable SIR system characteristics (e.g., L-band wavelength, HH polarization, and relatively large look angles), provided an environment conducive for subsurface imaging in Saudi Arabia during the SIR-A and SIR-B missions. These conditions are summarized as follows:

(1) The moisture content of the sand deposits is assumed to have been below the critical 1 percent level [7] during the SIR-A and SIR-B missions. Weather records indicate that the study areas had been without precipitation for at least six months prior to the Shuttle overflights in November 1981 and October 1984. Specifically, at the Al Labbah study area (Figure 2), the moisture level averaged 0.21 weight percent for sand samples collected at the surface and at two subsurface levels (three sites, three determinations per site) on the day of the SIR-B overpass. Such a diminished value describes a low loss medium that would permit the SIR signals to penetrate to a relatively deep depth without significant dispersion.

(2) The individual grains of the sand deposits were too small to scatter the large wavelength radar signals. Roth and Elachi [8] found that scattering losses are not prohibitive for subsurface penetration when individual grain sizes are smaller than one-tenth wavelength, and that scattering losses do not become appreciable until grain sizes become larger than one-fifth wavelength. With a SIR wavelength of 23.5 cm, the critical grain-size values are 2.35 and 4.70 cm, respectively. The mean grain size of surface and subsurface sand samples at the Al Labbah and Al Khunfah study sites (Figures 2 and 6) averaged 0.34 mm (n=9), or slightly more than one-thousandth of the wavelength.

(3) The quartose sand deposits were essentially devoid of clay minerals. Water-bearing minerals can severely attenuate radar signals, and thus drastically restrict signal penetration [9].

(4) The sand deposits did not contain buried inhomogeneities (e.g., coarse gravel layer, hardpan, duricrust) that would have prevented the radar signals from reaching a hidden landscape surface. If present, any subsurface backscatter would have been from the "suspended" interface and not from the buried geologic-terrain surface.

(5) The hidden landscape surfaces were radar rough, and they thus diffusely reflected the radar signals (Figure 1). If a buried substrate had been radar smooth, the propagated signals would have been specularly reflected away from the antenna, and there would have been no image evidence (i.e., signal modulation) of a subsurface landscape.

(6) The masking sand layers were thin enough to enable the radar signals to penetrate to a rough substrate and be reflected back through the low loss medium. If the surficial deposits had been excessively thick, the radar energy would have been converted to heat energy somewhere along the two-way travel path.

(7) With only sparse vegetation covering the sand deposits (<5 percent cover), there was an insufficient number of surface-point scatterers to diffusely reflect the propagated radar signals at the air-sand interface (Figures 4-5, 7-8). As a consequence, essentially all of the radar energy was available for penetration, with echo intensity being determined by the buried substrate.

SAND DEPOSITS AND BACKSCATTER ENHANCEMENT

The presence of a thin layer of dry sand could have enhanced the ability of SIR-A and SIR-B to image buried and partially buried substrates because of (1) refraction of the propagated radar beam at the air-sand interface, effectively producing a steeper or smaller incidence angle at the sand-bedrock interface (Figure 9), and (2) effective wavelength shortening in the penetrated medium. The smaller incidence angle and shorter wavelength would increase the backscatter, which would help compensate for any radar absorption losses in the sand and any specular reflection that occurred at the air-sand interface [10].

Without an overburden, the relationship between wavelength and incidence angle establishes the theoretical boundary between smooth and rough surfaces. The Rayleigh criterion considers a surface to be smooth if:

$$h < \frac{\lambda}{8 \cos \theta} \qquad (1)$$

where: h = average vertical relief of surface roughness (cm)

λ = operating radar wavelength (cm)

θ = incidence angle of the radar beam

By solving for h in Equation 1, the theoretical boundary of vertical relief separating radar-smooth and radar-rough surfaces is defined for a given wavelength and incidence angle. Accordingly, surfaces with a value of h less than the calculated value should produce dark image tones (radar-smooth surfaces), and surfaces with a value of h greater than the calculated value should be responsible for light image tones (radar-rough surfaces). For SIR-A with a wavelength of 23.5 cm and an incidence angle of 47^{o}, an average vertical relief of 4.3 cm is the theoretical boundary between smooth and rough surfaces.

However, given the condition of a sand-covered substrate, the Rayleigh criterion assumes the following form because of wave refraction [10,11]:

$$h' < \frac{\lambda'}{8 \cos \theta'} \qquad (2)$$

where: h' = apparent average vertical relief of subsurface roughness

$\lambda' = \lambda/\sqrt{\xi}$ with ξ being the complex dielectric constant of the penetrated medium

$\theta' = \arcsin([\sin \theta]/\sqrt{\xi})$

By using appropriate SIR-A values and $\xi = 2.5$, which was the mean complex dielectric constant[1] of surface and subsurface sand samples collected during the dry season at the Al Labbah Plateau study site (Figure 2), the parameters for Equation 2 are as follows: (1) the surface wavelength (λ) of 23.5 cm is reduced to a subsurface wavelength (λ') of 14.9 cm; (2) the surface incidence angle (θ) of 47° becomes 27.5° at the air-sand interface (θ'); and (3) the theoretical boundary between radar smooth and radar rough would have gone from 4.3 cm at the surface (h) to 2.1 cm at the subsurface (h'). Thus, with h' less than 2.1 cm, the rubble surface of the buried rocks of the Aruma Formation, for example, would clearly represent a radar-rough surface (Figure 3).

CONCLUSIONS

Our investigation has shown that L-band SIR images can delineate and characterize both concealed and obscured geologic terrains (i.e., hidden landscapes) that are not befit for detection by VIR sensors. Subsurface radar imaging was facilitated because the masking medium (overburden) and buried substrates possessed favorable physical and chemical characteristics that were amenable to radar penetration, refraction, and reflection during the SIR-A and SIR-B missions.

Although SIR-A and SIR-B provided only limited image coverage of Saudi Arabia, the unique radar views of several terrains do illustrate their potential for important applications in geology, hydrology, and archaeology. For example, the SIR images could be used effectively to assist the field geologist in mapping lithologic units and terrain features (e.g., drainage networks) in areas that are veneered by thin windblown sand

---

[1]The complex dielectric contrast (ξ) is a measure of a material's ability to conduct or reflect radar energy; as ξ increases, reflectivity increases, whereas conductivity or penetration decreases. At L-band wavelengths, most materials have an ξ of less than 8 when dry, but ξ may reach 80 when a material is extremely moist. The dielectric constant of a material increases almost linearly with increasing moisture content. Sand deposits would be expected to produce strong radar backscatter when damp, thus eliminating the possibility of signal penetration to a buried substrate.

deposits. A problem created by surficial masking is demonstrated on published 1:500,000-scale geology maps, where the level of detail is conspicuously generalized in sand-veneered areas because heavy reliance had to be placed on the interpretation of 1:60,000-scale panchromatic airphotos. We have found that in such areas, SIR interpretive data could be used to revise the existing maps by correcting errors and adding terrain information.

The ability of the SIR sensors to detect paleo-fluvial terrains has important applications in both hydrology and archaeology. For example, the relic alluvial valleys that formed during past humid periods could be favorable sites for shallow groundwater occurrence because they may contain large water-bearing beds that could be recharged if the paleodrainage systems are still in hydraulic communication with their original catchment areas in the Arabian Shield. The same paleodrainage systems are also considered to be favorable ecological niches for Stone Age and Neolithic settlements. During our survey work, for example, we discovered a number of MAR-TU stone-"kite" structures (animal traps) along the margins of many of the relic valleys (Figure 10); these structures were used from about 6,000 B.C. to 2,000 B.C. [12].

Being able to detect hidden landscapes with L-band SIR sensors expands the role of remote sensing as a tool for problem solving in the earth sciences. For Saudi Arabia and other countries that have been dominated by eolian depositional activities throughout the late Quaternary Period, the unique radar views will become fully exploitable when country-wide, L-band image coverage is provided by the NASA Earth Observing System that is planned to be operational by the late 1990's.

ACKNOWLEDGEMENTS

The SIR research program for Saudi Arabia had been made possible by funding provided by the King Abdulaziz City for Science and Technology and the National Aeronautics and Space Administration. Special thanks are due Charles Elachi and Martin Ruzek (Jet Propulsion Laboratory) for providing SIR images and supportive remote sensing data on a timely basis; Pat Chavez, JoAnn Bowell, and Lynda Bellisime (U.S. Geological Survey-Flagstaff, Arizona) for digital image processing support; Richard Larson (Environmental Research Institute of Michigan) for providing electrical-property measurements on collected sand samples; and helicopter pilots Michael Bell and John Jennings (Deputy Ministry for Mineral Resources) for their untiring efforts to satisfy our field-sampling objectives. We also wish to recognize the special contribution of Abdullah Al-Kadhi (Vice President, King Abdulaziz City for Science and Technology) for his encouragement and assistance in helping us solve a number of problems encountered during our ground surveys.

REFERENCES

1) Berlin, G.L., Tarabzouni, M.A., Sheikho, K.M., and Al-Naser, A.H., "SIR-A and Landsat MSS Observations of Eolian Sand Deposits on the Al Labbah Plateau, Saudi Arabia", Proceedings of the Nineteenth International Symposium on Remote Sensing of Environment, Environmental Research Institute of Michigan, Vol. 1, 1985, pp. 311-321.

2) Berlin, G.L., Tarabzouni, M.A., Al-Naser, A.H., Sheikho, K.M., and Larson, R.W., "SIR-B Subsurface Imaging of a Sand-Buried Landscape: Al Labbah Plateau, Saudi Arabia", IEEE Transactions on Geoscience and Remote Sensing, Vol. GE-24, July 1986, pp. 595-602.

3) Avery, T.E. and Berlin, G.L., "Nonphotographic Imaging Systems", Interpretation of Aerial Photographs, 4th ed., Macmillan, New York, 1985, pp. 141-233.

4) Sabins, F.F., Jr., "Radar Images", Remote Sensing Principles and Interpretation, 2nd ed., W.H. Freeman, New York, 1987, pp. 177-233.

5) UNESCO, Map of the World Distribution of Arid Regions and Explanatory Note, United Nations, Paris, 1977, 54 p. and 1:25 million-scale map.

6) Blom, R.G., "Effects of Variation in Look Angle and Wavelength in Radar Images of Volcanic and Aeolian Terrains, or Now You See It, Now You Don't", International Journal of Remote Sensing, Vol. 9, May 1988, pp. 945-965.

7) Blom, R.G., Crippen, R.E., and Elachi, C., "Detection of Subsurface Features in SEASAT Radar Images of Means Valley, Mojave Desert, California", Geology, Vol. 12, June 1984, pp. 346-349.

8) Roth, L.E., and Elachi, C., "Coherent Electromagnetic Losses by Scattering from Volume Inhomogeneities", IEEE Transactions on Antennas and Propagation, Vol. AP-23, Sept. 1975, pp. 674-675.

9) Schaber, G.G., McCauley, J.F., Breed, C.S., and Olhoeft, G.R., "Shuttle Imaging Radar: Physical Controls on Signal Penetration and Subsurface Scattering in the Eastern Sahara", IEEE Transactions on Geoscience and Remote Sensing, Vol. GE-24, July 1986, pp. 603-623.

10) Elachi, C., Roth, L.R., and Schaber, G.G., "Spaceborne Radar Subsurface Imaging in Hyperarid Regions", IEEE Transactions on Geoscience and Remote Sensing, Vol. GE-22, July 1984, pp. 383-388.

11) McCauley, J.F., Schaber, G.G., Breed, C.S., Grolier, M.J., Haynes, C.V., Issawi, B., Elachi, C., and Blom, R., "Subsurface Valleys and Geoarchaeology of the Eastern Sahara Revealed by Shuttle Radar", Science, Vol. 218, 3 Dec. 1982, pp. 1004-1020.

12) Zarins, J., "MAR-TU and the Land of Dilmun", Bahrain Through the Ages - The Archaeology, KPI Limited, London, 1986, pp. 233-250.

TABLE 1. Shuttle Imaging Radar Characteristics

Parameter	SIR-A	SIR-B
L-band wavelength	23.5 cm	23.5 cm
Polarization	HH	HH
Aperture Type	Synthetic	Synthetic
Correlation Processing	Optical	Optical & Digital
Look Angle - Center Swath	47^{o}	15^{o} to 60^{o}
Resolution - Center Swath		
Range (Across Track)	40 m	17 to 58 m
Azimuth (Along Track)	40 m	25 m
Swath Width	50 km	20 to 40 km
Shuttle Altitude	259 km	257 & 359 km
Launch Date	November 12, 1981	October 5, 1984
Mission Duration	2.4 Days	8.3 Days
Shuttle Vehicle	Columbia	Challenger

FIGURE CAPTIONS

Figure 1. Diagram showing two types of hidden landscapes that were detected by the SIR sensors, as indicated by the subsurface reflection profiles, but not by VIR sensors for the most part. Both VIR and SIR sensors can detect the exposed landscape. "Radar rough" pertains to the scale of a material's average vertical relief in relation to the wavelength and illumination geometry of the propagated radar energy that will cause diffuse reflection.

Figure 2. Multisensor view of the Al Labbah Plateau study site: (top) SIR-A image, 23.5-cm wavelength; (bottom) computer-enhanced Landsat TM band 3 image, 0.63 to 0.69-micrometer wavelength. Annotations are as follows: (A) a sand hill called Anbat, (B) a sand shadow (two wings) called Irq al Ubaytir, (C) the informally named Al Labbah sand sheet that was penetrated by both SIR-A and SIR-B beams, and (D) surface exposures of the Aruma Formation. Ground photographs of the Aruma Formation (location 1), penetrated sand sheet (location 2), and contact between the sand sheet and sand shadow (location 3) are shown in Figures 3-5.

Figure 3. Ground view of a typical outcrop of the Aruma Formation (location 1 in Figure 2). Numerous excavations reveal that this type of rubbly surface underlies the Al Labbah sand sheet. Notebook measures 14 x 22.5 cm.

Figure 4. Ground view of the Al Labbah sand sheet looking to the north (location 2 in Figure 2) that was penetrated by both SIR-A and SIR-B beams. Sand depth at helicopter is 83 cm. Shrub cover (Haloxylon salicornicum) is less than 1 percent.

Figure 5. Ground view from the Al Labbah sand sheet north to the southern wing of the Irq al Ubaytir sand shadow. Approximate contact is at the double arrow. In this view, the thickness of the sand sheet is about 30 cm, while that for the sand shadow is about 3.1 m. Shown is a Bedowin camp on the local high ground.

Figure 6. Multisensor view for a portion of the Al Khunfah Plateau and Wadi Nayyal paleodrainage system: (top) SIR-A image, 23.5-cm wavelength; (bottom) LFC panchromatic photograph, 0.5 to 0.7-micrometer wavelength. Aerial views of locations 1 and 2 are presented in Figures 7 and 8.

Figure 7. Aerial view of drift sand covering much of the Tawil sandstone (location 1 in Figure 6). Maximum measured sand depth in this view is 36 cm. Shrub cover (Haloxylon salicornicum) is less than 3 percent.

Figure 8. Aerial view of drift sand covering much of the Tawil sandstone and V-shaped paleowadi system (location 2 in Figure 6).

Figure 9. Diagram illustrating refraction of the propagated radar beam at the air-sand interface.

Figure 10. Aerial view of a MAR-TU animal trap that was used for the killing of orax, gazelle, wild goat, onager, and ostrich (all now extinct in Saudi Arabia). The animals were stampeded down the extensive guiding arms, through the neck, and into the enclosure. The circular hides concealed archers and spearmen.

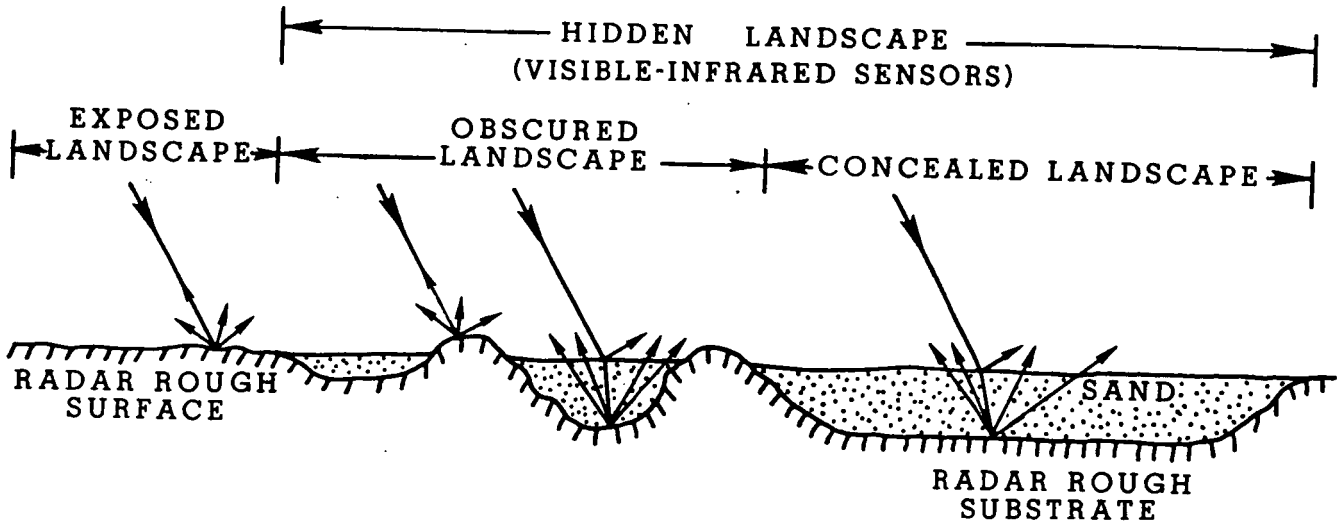
HIDDEN LANDSCAPE
(VISIBLE-INFRARED SENSORS)
EXPOSED LANDSCAPE
OBSCURED LANDSCAPE
CONCEALED LANDSCAPE
RADAR ROUGH SURFACE
SAND
RADAR ROUGH SUBSTRATE

Figure 1.

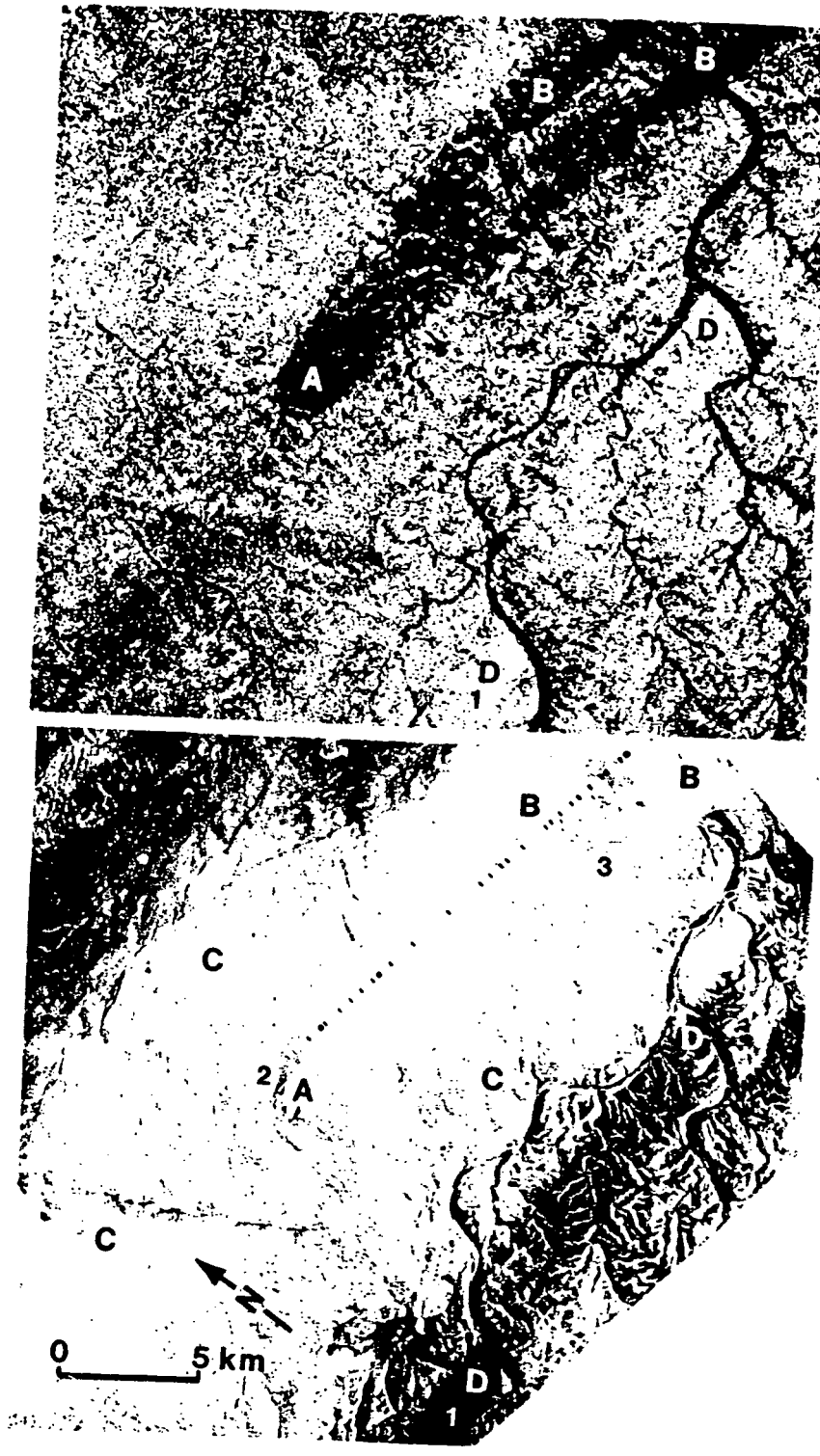

Figure 2.

Figure 3.

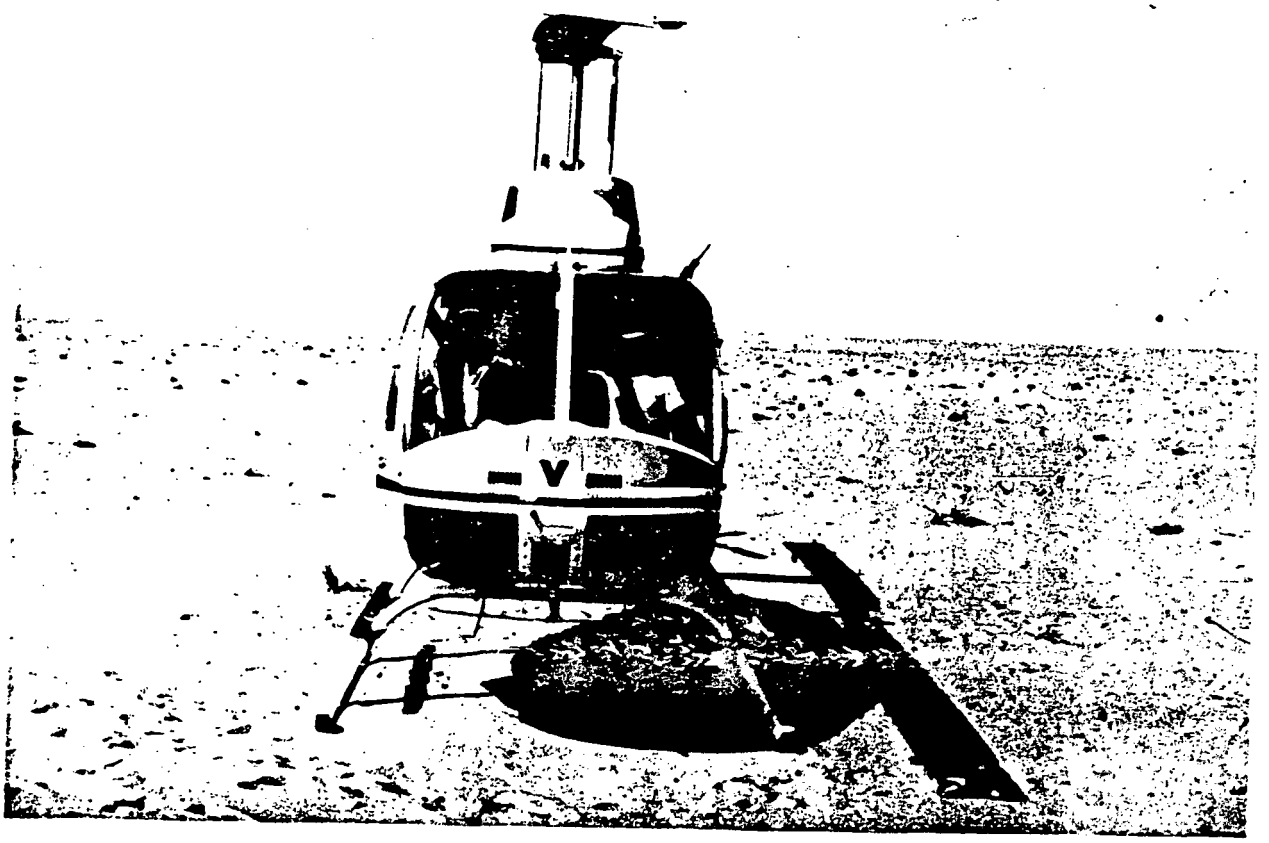

Figure 4.

Figure 5.

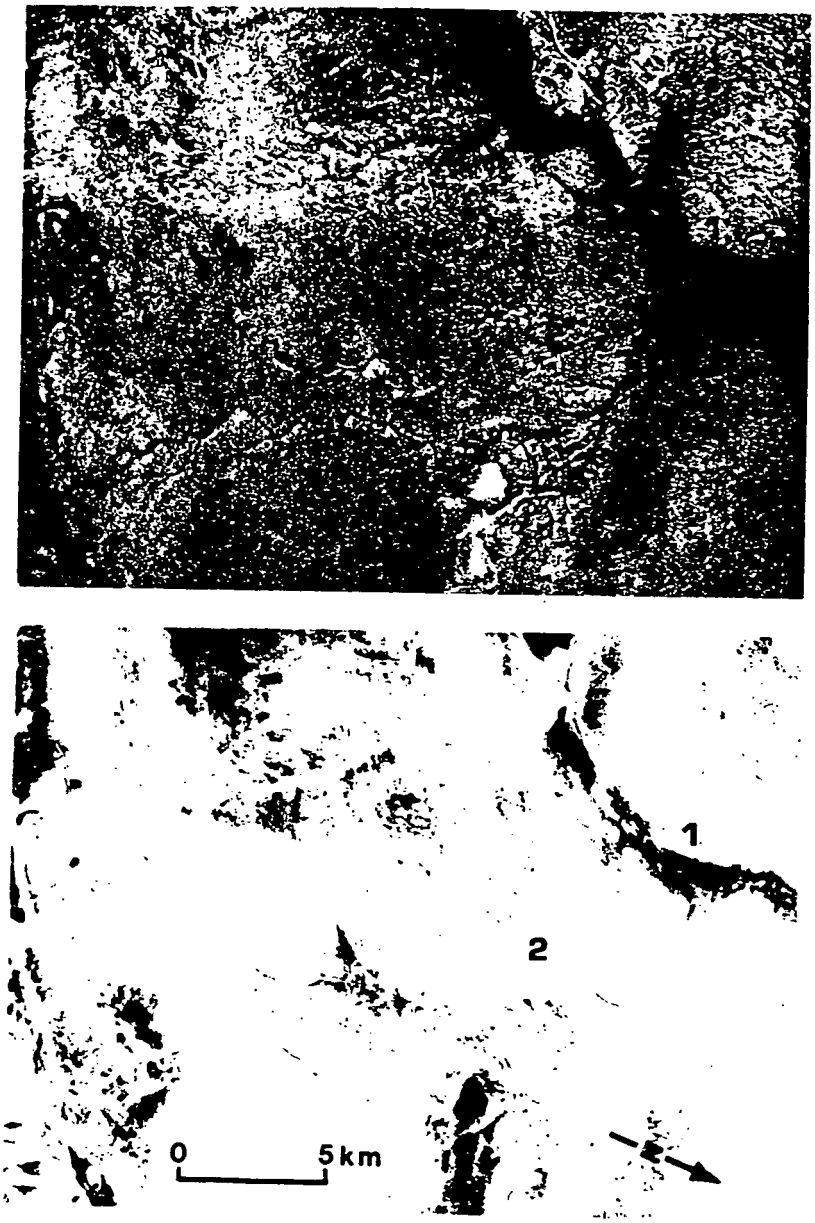

Figure 6.

Figure 7.

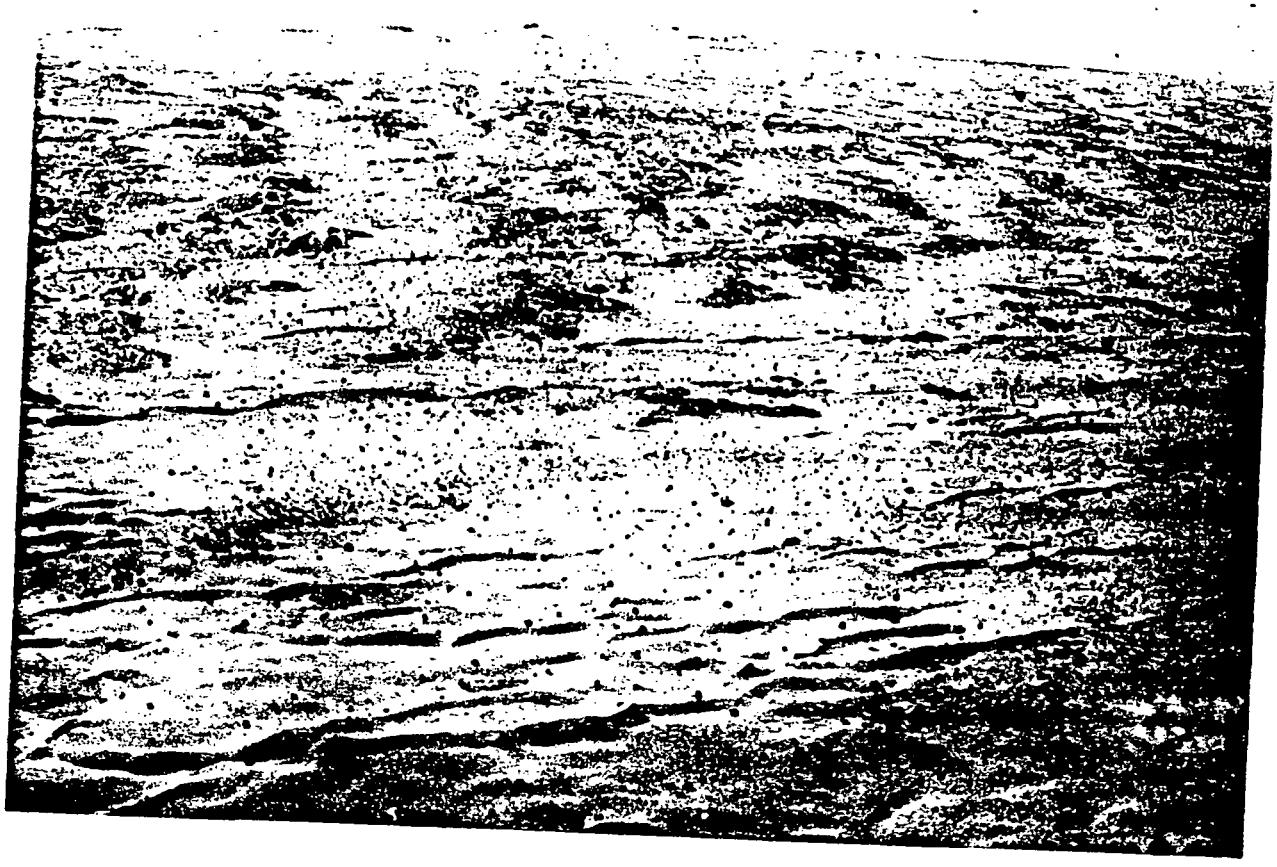

Figure 8.

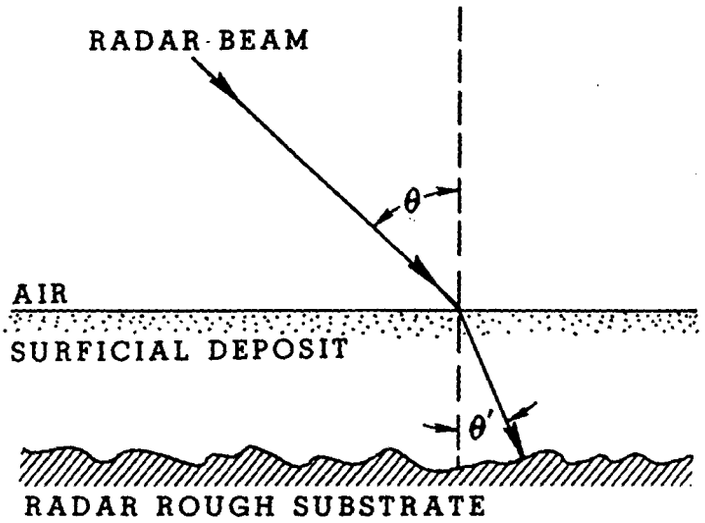

Figure 9.

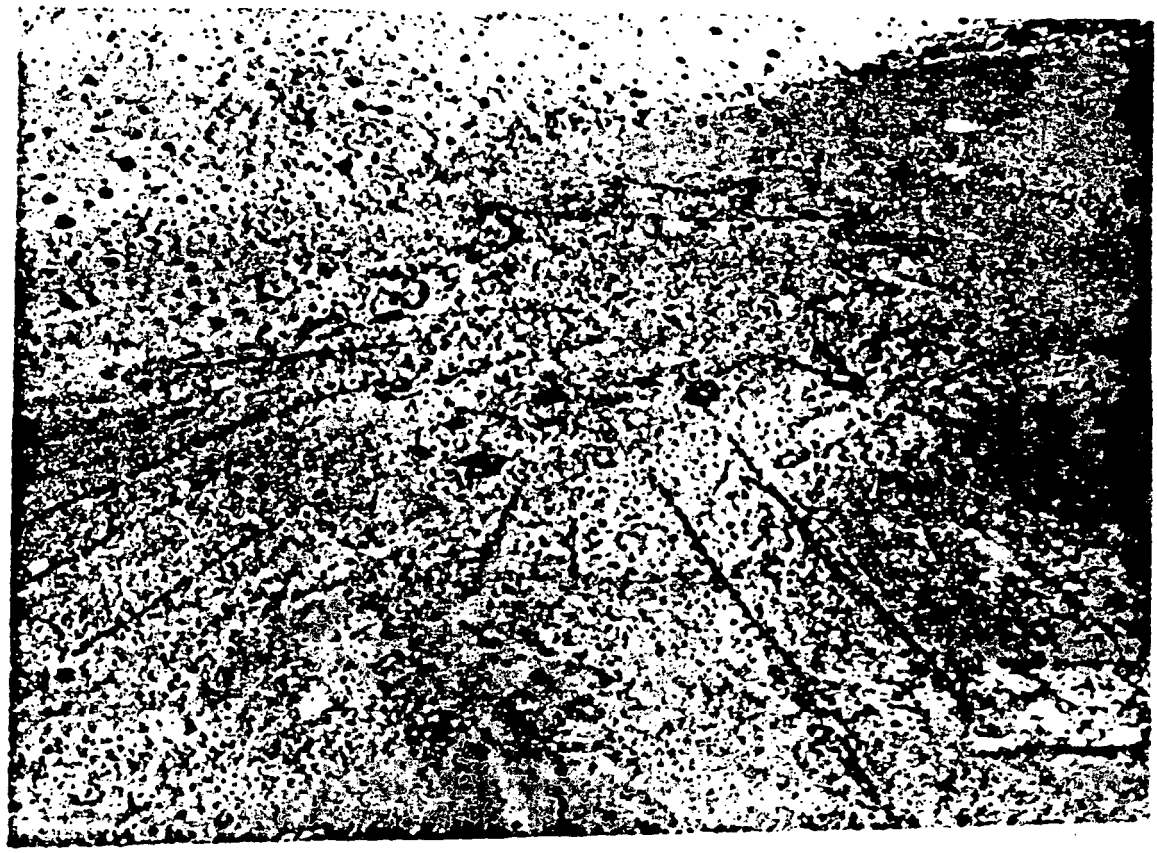

Figure 10.